Dalton Transactions

ROYAL SOCIETY OF CHEMISTRY

PAPER

View Article Online
View Journal | View Issue

Cite this: *Dalton Trans.*, 2024, **53**, 9554

Increasing the electron donation in a dinucleating ligand family: molecular and electronic structures in a series of $Co^{II}Co^{II}$ complexes†

Felix Depenbrock, Thomas Limpke, Anja Stammler, Jan Oldengott, Hartmut Bögge and Thorsten Glaser *

We have developed a family of dinucleating ligands with varying terminal donors to generate dinuclear peroxo and high-valent complexes and to correlate their stabilities and reactivities with their molecular and electronic structures as a function of the terminal donors. It appears that the electron-donating ability of the terminal donors is an important handle for controlling these stabilities and reactivities. Here, we present the synthesis of a new dinucleating ligand with potentially strong donating terminal imidazole donors. As Co^{II} ions are sensitive to variations in donor strength in terms of coordination number, magnetism, UV-Vis-NIR spectra, redox potentials, we probe the electron donation ability of this new ligand in $Co^{II}Co^{II}$ complexes in comparison to the parent $Co^{II}Co^{II}$ complexes with terminal pyridine donors and we synthesize the analogous $Co^{II}Co^{II}$ complexes with terminal 6-methylpyridines and methoxy-substituted pyridines. The molecular structures show indeed strong variations in coordination numbers and bond lengths. These differences in the molecular structures are reflected in the magnetic properties and in the d–d transitions demonstrating that the molecular structures remain intact upon dissolution. The redox potentials are analyzed with respect to the electron donation ability and are the only handle to observe an effect of the methoxy-substituted pyridines. All data taken together show the following order of electron donating ability for the terminal donors: 6-methylpyridines ≪ pyridines < methoxy-substituted pyridines ≪ imidazoles.

Received 25th March 2024,
Accepted 15th May 2024

DOI: 10.1039/d4dt00877d

rsc.li/dalton

Introduction

Nature frequently employs metalloproteins with a dinuclear active site and regulates their molecular and electronic structures and hence reactivity for function not only by the choice of the metal ions but also of the ligands.[1] A deeper understanding of the influence of the ligands on molecular and electronic structures and hence reactivity would be of benefit to use these biological catalysts as a blueprint for the development and optimization of molecular catalysts.[2] In this respect, we have developed a dinucleating ligand system[3] comprised of two tetradentate coordination compartments that vary in the terminal donors including carboxylates,[4] phenolates, and pyridines (Scheme 1).[5]

For example, we were able to model the frequently observed μ-1,2-peroxo $Fe^{III}Fe^{III}$ intermediate in dinuclear non-heme diiron proteins ($NHFe_2$) and to vary its reactivity: (i) using $susan^{6\text{-}Me}$, the stable complex $[(susan^{6\text{-}Me})\{Fe^{III}(\mu\text{-}1,2\text{-peroxo})(\mu\text{-}O)Fe^{III}\}]^{2+}$ was crystallized and protonated in solution to an unprecedented μ-1,2-hydroperoxo $Fe^{III}Fe^{III}$ species,[6] while (ii) using susan, $[(susan)\{Fe^{III}(\mu\text{-}1,2\text{-peroxo})(\mu\text{-}O)Fe^{III}\}]^{2+}$ is a reactive intermediate.[7] Similarly, $[(susan^{6\text{-}Me})\{Cu^{I}Cu^{I}\}]^{2+}$ reacts with O_2 to a reactive high-valent $\{Cu^{III}(\mu\text{-}O)_2Cu^{III}\}$ species, while $[(susan)\{Cu^{I}Cu^{I}\}]^{2+}$ reacts with O_2 to an also reactive $\{Cu^{II}\text{-}\mu\text{-}1,2\text{-peroxo-}Cu^{II}\}$ intermediate.[8] In dicobalt chemistry, the μ-1,2-peroxo complex $[(susan)\{Co^{III}(\mu\text{-}1,2\text{-peroxo})(\mu\text{-}OH)Co^{III}\}]^{3+}$ is stable and can only be reversibly deprotonated with a strong base in non-aqueous solution at low temperatures. In contrast, the oxidized $[(susan)\{Co^{III}(\mu\text{-}1,2\text{-superoxo})(\mu\text{-}OH)Co^{III}\}]^{4+}$ becomes deprotonated in aqueous solution above pH 2 and releases O_2 modelling the last step in water oxidation catalysis.[9] Independently of our work, interest in the reactivity of cobalt complexes has recently increased again.[10]

The detailed characterization and analysis of the molecular and electronic structures of our aforementioned complexes established that the reactivity of the dinuclear peroxo and

Lehrstuhl für Anorganische Chemie I, Fakultät für Chemie, Universität Bielefeld, Universitätsstrasse 25, D-33615 Bielefeld, Germany.
E-mail: thorsten.glaser@uni-bielefeld.de

†Electronic supplementary information (ESI) available: Experimental details crystal structure determination, FTIR spectra, NMR spectra, (pdf) X-ray crystallographic data (cif). CCDC 2341023–2341031. For ESI and crystallographic data in CIF or other electronic format see DOI: https://doi.org/10.1039/d4dt00877d

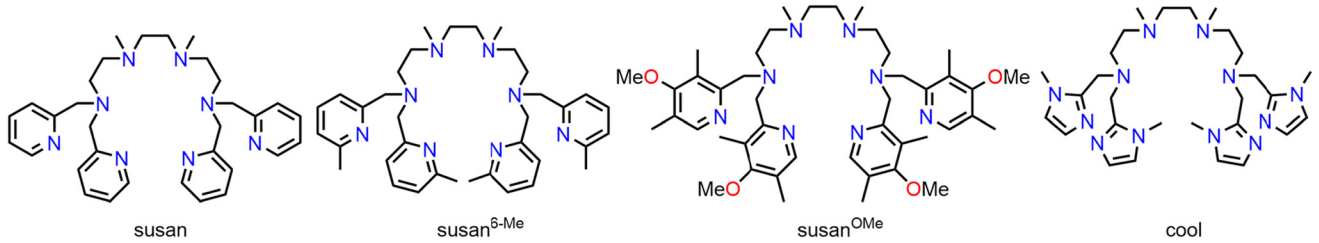

Scheme 1 The bis(tetradentate) dinucleating N_8 ligands used in this study.

high-valent complexes is controlled by the electron donation ability of the dinucleating ligands. Generally, the electron donation ability of a ligand can be tuned by the introduction of electron donating and electron withdrawing substituents quantified for aromatic substituents by the Hammett parameters.[11] A higher electron density in the ligand can on the one hand increase the electron donation of the ligand to the metal ion by σ- and π-donor interactions and on the other hand decrease the back-donation of electron density from the metal ion to the ligand by π-acceptor interactions. All three interactions (σ- and π-donor, π-acceptor) increase the strength and hence shorten the metal–ligand bond. However, they do not correlate with the spectrochemical series. The latter classifies the ligands in their ability to induce a ligand-field splitting ranging from "weak ligands" to "strong ligands". Although both π-donor and π-acceptor ligands increase the strength of the metal–ligand bond, π-donors are "weak ligands" and π-acceptors are "strong ligands".

The ligand susan$^{6\text{-Me}}$ is less electron donating than the ligand susan due to the longer M–$N^{6\text{-Me-py}}$ bonds enforced by the sterical demand of the 6-methyl substituents. In order to further tune the reactivity of peroxo intermediates and to stabilize high-valent intermediates, we intend to increase the electron donation capabilities of our dinucleating ligand system and initially used phenolate donors that are both strong σ- and π-donors. However, although those complexes are oxidized at relatively low potentials, the oxidation is not metal-centered but ligand-centered resulting in coordinated phenoxyl radicals.[5,12] More recently, we reported the synthesis of the ligand susan^{OMe},[13] a substitution pattern that was already successfully employed with tris(2-pyridylmethyl)amine (tpa) ligands.[14] This substitution increases the electron density in the pyridine π-system reducing the π-acceptor character.

Considering that nature uses imidazole ligands in form of the amino acid histidine and not pyridine donors, it is interesting to consider the substitution of the pyridine donors in susan by imidazole donors. Here, we report the synthesis of the ligand cool that employs methylimidazole as terminal donors (Scheme 1). Imidazoles are considered as π-donor ligands, whereas pyridines are considered to be π-acceptor ligands.[15] A chemical intuitive interpretation is that in imidazoles the six π electrons are shared only over five atoms instead of six atoms in pyridines so that the higher electron density per atom facilitates π-donor interaction and increases the energy of the π-donor orbitals. Therefore, the electron donation capability of the ligand cool should be stronger than of the ligands susan and susan^{OMe}. With the ligand susan, we already synthesized a series of dinuclear $Co^{II}Co^{II}$ complexes, namely $[(susan)\{Co^{II}(CH_3CN)_2\}_2]^{4+}$, $[(susan)\{Co^{II}Cl\}_2]^{2+}$, $[(susan)\{Co^{II}Br\}_2]^{2+}$, and $[(susan)\{Co^{II}(\mu\text{-}OH)Co^{II}\}]^{3+}$.[16] Here we employ the new ligand cool as well as the ligands susan^{OMe} and susan$^{6\text{-Me}}$ to extend this series of dinuclear $Co^{II}Co^{II}$ complexes and to evaluate the influence of the terminal nitrogen donors and the exogenous ligands on the molecular structures evaluated by single-crystal X-ray diffraction and on the electronic structures evaluated by magnetism, UV-Vis-NIR spectroscopy, and electrochemistry. These investigations result in the following sequence of electron donation ability: susan$^{6\text{-Me}}$ ≪ susan < susan^{OMe} ≪ cool.

Experimental section

Synthesis of compounds

Solvents and starting materials were of the highest commercially available purity and used as received except for CH_3CN, which was dried according to standard procedures.[17] Tetramine **1** (= 4,7-dimethyl-1,4,7,10-tetrazadecane) was synthesized by a modified literature procedure.[18] The ligands susan$^{6\text{-Me}}$ (ref. 19) and susan^{OMe} (ref. 13) were synthesized according to the procedures reported previously. Although we experienced no difficulties, perchlorate salts are potentially hazardous and should only be handled in small quantities and with adequate precautions. The assignments of the NMR resonances in all products were supported by 2D COSY, HMBC, and HMQC spectroscopy and the numbering was done according to the numbering scheme in Fig. S2 + S3.†

4,7-Dimethyl-1,1,10,10-tetra((1-methyl-1*H*-imidazol-2-yl)methyl)-1,4,7,10-tetraazadecane (cool). Solid $NaBH(OAc)_3$ (39.98 g, 188.6 mmol, 9 equiv.) was added to a solution of 1-methyl-1*H*-imidazole-2-carbaldehyde (10.32 g, 93.72 mmol, 4.5 equiv.) and tetramine **1** (3.63 g, 20.8 mmol, 1 equiv.) in 1,2-dichloroethane (1,2-DCE, 200 mL) at 0 °C. After stirring the reaction mixture for 3 d, the reaction was quenched with water (20 mL) and aqueous KOH (10 M, 200 mL) was added. The layers were separated, and the aqueous layer was extracted with CH_2Cl_2 (4 × 100 mL). The combined organic fractions were washed with aqueous KOH (10 M, 100 mL) and brine (100 mL), dried

over $MgSO_4$, and the solvent was removed under reduced pressure providing a yellow oil. This oil was dissolved in i-PrOH (50 mL) and treated with HCl (6 N in i-PrOH, 250 mL) resulting in the deposition of an off-white solid that was separated by filtration, washed with HCl (6 N in i-PrOH, 2 × 50 mL), and then dissolved in aqueous KOH (10 M, 300 mL). Extraction with CH_2Cl_2 (3 × 100 mL), drying of the combined organic layers ($MgSO_4$), and removal of the solvent under reduced pressure provided a yellowish oil. Addition of Et_2O (50 mL) caused the deposition of a colorless solid, which was collected by filtration, washed with Et_2O, and dried under reduced pressure. Yield: 6.53 g (11.9 mmol, 57%). IR (KBr): $\tilde{\nu}$/cm^{-1} = 3401 m br, 3104 m, 2975 m, 2985 m, 2887 w, 2825 s, 2802 s, 2721 w, 1638 w, 1500 s, 1471 m, 1452 m, 1412 m, 1370 m, 1339 w, 1302 w, 1283 s, 1255 w, 1245 w, 1214 w, 1199 w, 1141 m, 1113 m, 1089 m, 1050 m, 986 m, 971 m, 945 m, 921 w, 853 w, 815 w, 768 s, 714 m, 695 w, 659 m, 628 m, 589 w. ESI-MS (CH_3CN): m/z = 551.4 [cool + H]$^+$, 573.4 [cool + Na]$^+$. ^{1}H NMR (500 MHz, $CDCl_3$): δ/ppm = 6.88 (d, ^3J = 1.2 Hz, 4H, H9), 6.78 (d, ^3J = 1.2 Hz, 4H, H8), 3.69 (s, 8H, H5), 3.48 (s, 12H, H7), 2.68 (t, ^3J = 6.5 Hz, 4H, H4), 2.44 (t, ^3J = 6.5 Hz, 4H, H3), 2.37 (s, 4H, H1), 2.08 (s, 6H, H2). ^{13}C{^{1}H} NMR (125 MHz, $CDCl_3$): δ/ppm = 145.4 (C6), 127.3 (C9), 121.6 (C8), 55.7 (C3), 55.1 (C1), 51.1 (C4), 50.6 (C5), 42.1 (C2), 32.6 (C7). Anal. Calcd for cool·0.33H_2O, $C_{28}H_{46.66}N_{12}O_{0.33}$: C 60.40, H 8.45, N 30.19. Found: C 60.53, H 8.47, N 29.95.

[(susan$^{6\text{-Me}}$){Co^{II}(CH$_3$CN)$_2$}$_2$](ClO$_4$)$_4$·H$_2$O. A solution of susan$^{6\text{-Me}}$ (99 mg, 166 μmol) in CH_3CN (5 mL) was added to a solution of $Co(ClO_4)_2·6H_2O$ (123 mg, 336 μmol) in CH_3CN (5 mL). The resulting purple solution was stirred for 10 minutes followed by filtration. Diffusion of Et_2O into the filtrate led to the deposition of purple crystals suitable for single-crystal X-ray diffraction. The crystals were filtered off, washed three times with Et_2O, and dried under reduced pressure. Yield: 59 mg (46 μmol, 28%). IR (KBr): $\tilde{\nu}$/cm^{-1} = 3430 m br, 3082 w, 3003 w, 2977 w, 2938 w, 2284 w, 2014 w, 1609 m, 1577 w, 1468 m, 1370 w, 1276 w, 1091 s, 954 w, 854 w, 795 w, 782 w, 625 s. ESI-MS (CH_3CN): m/z = 270.4 {[(susan$^{6\text{-Me}}$)Co$^{II}_2$]ClO$_4$}$^{3+}$, 455.1 {[(susan$^{6\text{-Me}}$)Co$^{II}_2$](ClO$_4$)$_2$}$^{2+}$. Anal. Calcd for [(susan$^{6\text{-Me}}$){Co^{II}(CH$_3$CN)$_2$}$_2$](ClO$_4$)$_4$·H_2O, $C_{44}H_{64}N_{12}O_{17}Cl_4Co_2$: C 40.88, H 4.99, N 13.00. Found: C 40.69, H 5.14, N 12.80.

[(susan$^{6\text{-Me}}$){Co^{II}(μ-OH)$_2$Co^{II}}](ClO$_4$)$_2$·1.5H$_2$O. A solution of susan$^{6\text{-Me}}$ (201 mg, 338 μmol) in MeOH (9 mL) was added to a solution of $Co(ClO_4)_2·6H_2O$ (246 mg, 672 μmol) in MeOH (18 mL) providing a purple solution. Addition of NEt_3 (115 mg, 1.14 mmol) resulted in a color change to green. Storing at −20 °C led to the deposition of green crystals suitable for single-crystal X-ray diffraction. The crystals were filtered off, washed three times with H_2O and Et_2O, and dried under reduced pressure. Yield: 152 mg (161 μmol, 48%). IR (KBr): $\tilde{\nu}$/cm^{-1} = 3436 m br, 3083 w, 2975 w, 2918 w, 2867 w, 2014 w, 1604 m, 1577 w, 1464 m, 1431 w, 1384 w, 1350 w, 1291 w, 1092 s, 956 w, 850 w, 781 m, 624 m. ESI-MS (CH_3CN): m/z = 364.2 [(susan$^{6\text{-Me}}$)Co$^{II}_2$O]$^{2+}$. Anal. Calcd for [(susan$^{6\text{-Me}}$){Co^{II}(μ-OH)$_2$Co^{II}}](ClO$_4$)$_2$·1.5H_2O, $C_{36}H_{55}N_8O_{11.5}Cl_2Co_2$: C 44.46, H 5.70, N 11.52. Found: C 44.31, H 5.47, N 11.46.

[(susan^{OMe}){Co^{II}Cl}$_2$](ClO$_4$)$_2$·3MeOH. A solution of susan^{OMe} (101 mg, 131 μmol) in EtOH (12 mL) was added to a solution of $Co(ClO_4)_2·6H_2O$ (47 mg, 130 μmol) and $CoCl_2·6H_2O$ (31 mg, 130 μmol) in MeOH (28 mL) providing a blue solution. The solution was stirred for 10 minutes followed by filtration. Slow evaporation of the solvent at room temperature led to the deposition of bluish green crystals suitable for single-crystal X-ray diffraction. The crystals were filtered off, washed three times with Et_2O, and dried under reduced pressure. Yield: 110 mg (88 μmol, 67%). IR (KBr): $\tilde{\nu}$/cm^{-1} = 3435 m br, 2931 w, 3877 w, 2009 w, 1603 m, 1575 w, 1481 m, 1404 m, 1385 w, 1370 w, 1271 m, 1429 w, 1227 w, 1122 s, 1090 s, 1046 m, 994 m, 943 w, 886 w, 847 w, 789 w, 773 w, 624 m. ESI-MS (CH_3CN): m/z = 479.3 [(susan^{OMe}){Co^{II}Cl}$_2$]$^{2+}$. Anal. Calcd for [(susan^{OMe}){Co^{II}Cl}$_2$](ClO$_4$)$_2$·3MeOH, $C_{47}H_{78}N_8O_{15}Cl_4Co_2$: C 44.99, H 6.27, N 8.93. Found: C 44.71, H 6.24, N 8.83.

[(susan^{OMe}){Co^{II}Br}$_2$](ClO$_4$)$_2$·3MeOH. A solution of susan^{OMe} (99 mg, 128 μmol) in MeOH (20 mL) was added to a solution of $Co(ClO_4)_2·6H_2O$ (47 mg, 130 μmol) and $CoBr_2$ (28 mg, 130 μmol) in MeOH (25 mL) providing a blue solution. The solution was stirred for 5 minutes followed by filtration. Slow evaporation of the solvent at room temperature led to the deposition of bluish green crystals suitable for single-crystal X-ray diffraction. The crystals were filtered off, washed three times with Et_2O, and dried under reduced pressure. Yield: 90 mg (67 μmol, 52%). IR (KBr): $\tilde{\nu}$/cm^{-1} = 3440 m br, 2929 w, 2877 w, 2008 w, 1603 m, 1577 w, 1481 m, 1403 m, 1385 w, 1370 w, 1358 w, 1272 m, 1249 w, 1122 s, 1091 s, 1047 w, 994 m, 944 w, 886 w, 848 w, 789 w, 772 w, 624 m. ESI-MS (CH_3CN): m/z = 524.1 [(susan^{OMe}){Co^{II}Br}$_2$]$^{2+}$. Anal. Calcd for [(susan^{OMe}){Co^{II}Br}$_2$](ClO$_4$)$_2$·3MeOH, $C_{47}H_{78}N_8O_{15}Br_2Cl_2Co_2$: C 42.01, H 5.85, N 8.34. Found: C 41.91, H 5.89, N 8.29.

[(susan^{OMe}){Co^{II}(μ-OH)Co^{II}}](ClO$_4$)$_3$·1.5H$_2$O. A solution of susan^{OMe} (102 mg, 132 μmol) in CH_3CN (8 mL) was added to a solution of $Co(ClO_4)_2·6H_2O$ (98 mg, 268 μmol) in CH_3CN (8 mL) providing a purple solution. Addition of NEt_3 (43 mg, 428 μmol) resulted in a color change to green. The solution was stirred for 10 minutes followed by filtration. Diffusion of Et_2O into the filtrate led to the deposition of green crystals suitable for single-crystal X-ray diffraction. The crystals were filtered off, washed three times each with Et_2O, and dried under reduced pressure. Yield: 110 mg (89 μmol, 68%). IR (KBr): $\tilde{\nu}$/cm^{-1} = 3435 s br, 2932 w, 2877 w, 2032 w, 1604 m, 1578 w, 1482 m, 1405 m, 1384 w, 1369 w, 1359 w, 1302 w, 1269 m, 1252 w, 1227 w, 1201 w, 1122 s, 1109 s, 1093 s, 1047, 993 m, 943 w, 910 w, 884 w, 844 w, 801 w, 770 w, 625 m, 520 w. ESI-MS (CH_3CN): m/z = 502.2 {[(susan^{OMe}){Co^{II}(μ-OH)Co^{II}}$_2$]ClO$_4$}$^{2+}$, 1103.1 {[(susan^{OMe}){Co^{II}(μ-OH)Co^{II}}$_2$](ClO$_4$)$_2$}$^+$. Anal. Calcd for [(susan^{OMe}){Co^{II}(μ-OH)Co^{II}}](ClO$_4$)$_3$·1.5H_2O, $C_{47}H_{70}N_8O_{18.5}Cl_3Co_2$: C 42.92, H 5.73, N 9.10. Found: C 42.89, H 5.89, N 8.91.

[(cool){Co^{II}(CH$_3$CN)}$_2$](ClO$_4$)$_4$·CH$_3$CN. A solution of cool (50 mg, 91 μmol) in CH_3CN (4 mL) was added to a solution of $Co(ClO_4)_2·6H_2O$ (66 mg, 180 μmol) in CH_3CN (4 mL) providing a purple solution. The solution was stirred for 10 minutes followed by filtration. Diffusion of MeOH into the filtrate led to

the deposition of purple crystals suitable for single-crystal X-ray diffraction. The crystals were filtered off, washed three times with MeOH and Et_2O, and dried under reduced pressure. Yield: 86 mg (75 μmol, 80%). IR (KBr): $\tilde{\nu}/cm^{-1}$ = 3438 m br, 3152 m, 3133 m, 2995 w, 2959 w, 2888 w, 2314 w, 2285 w, 2252 w, 2024 w, 1632 w, 1554 w, 1507 m, 1477 w, 1467 w, 1457 w, 1357 w, 1317 w, 1289 w, 1165 m, 1155 m, 1097 s, 1043 m, 1001 w, 975 w, 946 w, 844 w, 784 w, 756 w, 679 w, 657 w, 624 s. ESI-MS (CH_3CN): m/z = 369.1 $[(cool)\{Co^{II}Cl\}_2]^{2+}$. Anal. Calcd for $[(cool)\{Co^{II}(CH_3CN)\}_2](ClO_4)_4\cdot CH_3CN$, $C_{34}H_{55}N_{15}O_{16}Cl_4Co_2$: C 34.33, H 4.66, N 17.66. Found: C 34.53, H 4.77, N 17.60.

$[(cool)\{Co^{II}Cl\}_2](ClO_4)_2$. A solution of cool (100 mg, 182 μmol) in MeOH (40 mL) was added to a solution of $Co(ClO_4)_2\cdot 6H_2O$ (66 mg, 180 μmol) and $CoCl_2\cdot 6H_2O$ (43 mg, 181 μmol) in MeOH/EtOH (20 mL/20 mL) providing a purple solution. The solution was stirred for 10 minutes followed by filtration. Slow evaporation of the solvent at room temperature led to the deposition of purple crystals suitable for single-crystal X-ray diffraction. The crystals were filtered off, washed three times with Et_2O, and dried under reduced pressure. Yield: 124 mg (132 μmol, 73%). IR (KBr): $\tilde{\nu}/cm^{-1}$ = 3437 m br, 3155 w, 3132 w, 2976 w, 2922 w, 2877 w, 2013 w, 1627 w, 1551 w, 1508 m, 1463 m, 1423 w, 1359 w, 1309 w, 1286 m, 1161 m, 1121 s, 1098 s, 1080 s, 1005 w, 991 w, 970 w, 945 w, 931 w, 853 w, 841 w, 822 w, 773 w, 743 w, 679 w, 657 w, 624 s. ESI-MS (CH_3CN): m/z = 369.1 $[(cool)\{Co^{II}Cl\}_2]^{2+}$, 773.2 $\{[(cool)\{Co^{II}Cl\}_2]Cl\}^{+}$. Anal. Calcd for $[(cool)\{Co^{II}Cl\}_2](ClO_4)_2$ $C_{28}H_{46}N_{12}O_8Cl_4Co_2$: C 35.84, H 4.94, N 17.91. Found: C 35.64, H 4.98, N 17.62.

$[(cool)\{Co^{II}Br\}_2](ClO_4)_2\cdot MeOH$. A solution of cool (100 mg, 182 μmol) in MeOH (40 mL) was added to a solution of $Co(ClO_4)_2\cdot 6H_2O$ (66 mg, 180 μmol) and $CoBr_2$ (40 mg, 183 μmol) in MeOH (40 mL) providing a purple solution. The solution was stirred for 10 minutes followed by filtration. Slow evaporation of the solvent at room temperature led to the deposition of purple crystals suitable for single-crystal X-ray diffraction. The crystals were filtered off, washed three times with Et_2O, and dried under reduced pressure. Yield: 131 mg (127 μmol, 70%). IR (KBr): $\tilde{\nu}/cm^{-1}$ = 3435 m br, 3156 w, 3134 w, 2977 w, 2920 w, 2876 w, 2015 w, 1628 w, 1551 w, 1506 m, 1463 w, 1422 w, 1358 w, 1285 m, 1161 m, 1122 s, 1097 s, 1085 s, 990 w, 970 w, 945 w, 931 w, 850 w, 821 w, 764 w, 741 w, 678 w, 657 w, 624 s. ESI-MS (CH_3CN): m/z = 413.1 $[(cool)\{Co^{II}Br\}_2]^{2+}$, 391.1 $[(cool)\{Co^{II}Br\}\{Co^{II}Cl\}]^{2+}$, 369.1 $[(cool)\{Co^{II}Cl\}_2]^{2+}$. Anal. Calcd for $[(cool)\{Co^{II}Br\}_2](ClO_4)_2\cdot MeOH$, $C_{29}H_{50}N_{12}O_9Br_2Cl_2Co_2$: C 32.88, H 4.76, N 15.87. Found: C 32.75, H 4.65, N 15.85.

$[(cool)\{Co^{II}(\mu\text{-}OH)Co^{II}\}](BPh_4)_2(OTf)\cdot 1.5CH_3CN\cdot 0.5H_2O$. A solution of cool (50 mg, 91 μmol) in CH_3CN (5 mL) was added to a solution of $Co(OTf)_2\cdot 7H_2O$ (88 mg, 182 μmol) in CH_3CN (10 mL) providing a purple solution. Addition of NEt_3 (27 mg, 267 μmol) resulted in a color change to blue. Solid $KBPh_4$ (101 mg, 281 μmol) was added and the resulting suspension was stirred for 90 minutes followed by filtration. Diffusion of Et_2O into the filtrate led to the deposition of blue crystals suitable for single-crystal X-ray diffraction. The crystals were filtered off, washed three times with Et_2O, and dried under reduced pressure. Yield: 30 mg (20 μmol, 22%). IR (KBr): $\tilde{\nu}/cm^{-1}$ = 3447 m br, 3144 w, 3126 w, 3055 m, 3041 w, 2996 w, 2985 w, 2927 w, 2876 w, 2250 w, 1946 w, 1889 w, 1829 w, 1761 w, 1631 m, 1580 m, 1550 w, 1508 s, 1479 w, 1428 m, 1384 w, 1373 w, 1355 w, 1286 s, 1256 s, 1223 w, 1158 s, 1119 w, 1086 w, 1032 s, 985 w, 970 w, 962 w, 938 w, 846 w, 836 w, 734 s, 706 s, 676 w, 655 w, 639 s, 614 m, 606 m, 572 w, 519 m, 478 w. ESI-MS (CH_3CN): m/z = 369.1 $[(cool)\{Co^{II}Cl\}_2]^{2+}$. Anal. Calcd for $[(cool)\{Co^{II}(\mu\text{-}OH)Co^{II}\}](BPh_4)_2(OTf)\cdot 1.5CH_3CN\cdot 0.5H_2O$, $C_{80}H_{92.5}N_{13.5}O_{4.5}B_2Co_2F_3S$: C 62.24, H 6.04, N 12.25, S 2.08. Found: C 62.22, H 6.13, N 12.20, S 1.97.

Crystal structure determination

Single-crystals were removed from the mother liquor, coated with oil, and measured at 100(2) K. For crystals of $[(susan^{6\text{-}Me})\{Co^{II}(\mu\text{-}OH)_2Co^{II}\}](ClO_4)_2\cdot MeOH$ a Bruker X8 prospector ultra three-circle diffractometer with 4K CCD detector, CuKα radiation, and Quazar™ Montel multilayer optics was used. Other crystals were measured on a Bruker KAPPA APEX II four-circle diffractometer equipped with 4K CCD detector. On this device, CuKα radiation with Quazar™ Montel multilayer optics was used to measure crystals of $[(susan^{6\text{-}Me})\{Co^{II}(CH_3CN)_2\}_2](ClO_4)_4$ and MoKα radiation with a focusing graphite monochromator for all other compounds. Empirical absorption corrections using equivalent reflections were performed with the programs SADABS 2012/1 for crystals of $[(cool)\{Co^{II}(CH_3CN)\}_2](ClO_4)_4\cdot 2CH_3CN$ and SADABS-2016/2 for all other data sets.[20] The structures were solved and refined *vs.* F^2 with the programs SHELXS/T/L[21,22] using OLEX2.[22] Crystal data and details concerning data collections and structure refinements are given in Table S1.†

Hydrogen atoms were found and refined for all bridging hydroxo-groups, all other hydrogen atoms were generated. All crystal structures contain counter ions of which several showed disorder to various extend. This disorder was resolved when possible and refined using the appropriate constraints. Crystal structures of $[(susan^{OMe})\{Co^{II}Cl\}_2](ClO_4)_2\cdot 3MeOH$ and $[(susan^{OMe})\{Co^{II}Br\}_2](ClO_4)_2\cdot 3MeOH$ are isostructural. Both contain solvent accessible voids, a channel along the 2_1 screw axis and a smaller void (Fig. S5†). The scattering contribution of the disordered MeOH molecules inside the voids was masked using OLEX2.[23,24] Two CH_3CN solvent molecules in $[(susan^{OMe})Co^{II}(\mu\text{-}OH)Co^{II}](ClO_4)_3\cdot 3CH_3CN$ suffered from substantial disorder and were also masked using the OLEX2 routine.[23,24]

$[(susan^{6\text{-}Me})\{Co^{II}(CH_3CN)_2\}_2](ClO_4)_4$ and $[(cool)\{Co^{II}(CH_3CN)\}_2](ClO_4)_4\cdot 2CH_3CN$ both crystallize with one half molecule in the asymmetric unit with the second half generated by a center of inversion. $[(susan^{6\text{-}Me})\{Co^{II}(\mu\text{-}OH)_2Co^{II}\}](ClO_4)_2\cdot MeOH$, $[(susan^{OMe})\{Co^{II}Cl\}_2](ClO_4)_2\cdot 3MeOH$, $[(susan^{OMe})\{Co^{II}Br\}_2](ClO_4)_2\cdot 3MeOH$ $[(susan^{OMe})Co^{II}(\mu\text{-}OH)Co^{II}](ClO_4)_3\cdot 3CH_3CN$, $[(cool)\{Co^{II}Cl\}_2](ClO_4)_2$, $[(cool)\{Co^{II}Br\}_2](ClO_4)_2$, and $[(cool)Co^{II}(\mu\text{-}OH)Co^{II}](BPh_4)_2(CF_3SO_3)\cdot 2CH_3CN$ all crystallize with a whole molecule in the asymmetric unit.

CCDC numbers (Table S1†) contain the supplementary crystallographic data for this paper.

Other physical measurements

Infrared spectra (400–4000 cm^{-1}) of solid samples were recorded on a Bruker Vertex 70 as KBr disks. ESI mass spectra were recorded on a Bruker Esquire 3000 ion trap mass spectrometer equipped with a standard ESI source. ^{1}H and $^{13}C\{^{1}H\}$ NMR spectra were measured on a Bruker Avance III 500 HD or a Bruker Avance III 300 spectrometer using the solvent as an internal standard. UV-Vis-NIR absorption spectra were measured on a JASCO V770 spectrophotometer at 20 °C. Cyclic and square-wave voltammograms (CVs and SWs) were measured by use of an EG&G potentiostat/galvanostat 273A on N_2-flushed solutions containing 0.1 M $TBAPF_6$ as supporting electrolyte in a conventional electrochemical cell. The working electrode was a GC electrode, the counter electrode was a platinum wire, and the reference electrode was Ag/0.01 M $AgNO_3$/CH_3CN. The potentials are referenced *versus* the ferrocenium/ferrocene (Fc^+/Fc) couple used as an internal standard. SWs have been recorded with typical frequency 60 Hz. CVs were routinely measured with scan rates of 200 mV s^{-1}. Magnetic susceptibility data were measured on powdered samples in the temperature range 2–300 K by using a SQUID magnetometer (Quantum Design MPMS XL-7 EC) with a field of 1.0 T. Variable-temperature variable-field (VTVH) measurements were performed in various static fields (1–7 T) in the range 2–10 K with the magnetization equidistantly sampled on a $1/T$ temperature scale. For calculations of the molar magnetic susceptibilities, χ_m, the measured susceptibilities were corrected for the underlying diamagnetism of the sample holder and the sample by using tabulated Pascal's constants.

Results and discussion

Synthesis

In analogy to the other N_8 ligands of our dinucleating ligand system,[5,13,19] the ligand cool was synthesized by a reductive amination[25] of tetramine **1** with 1-methyl-1*H*-imidazole-carbaldehyde (Scheme 2). Reacting cool with $Co(ClO_4)_2{\cdot}6H_2O$ in CH_3CN resulted in $[(cool)\{Co^{II}(CH_3CN)\}_2](ClO_4)_4$. The reaction of cool with $Co(ClO_4)_2{\cdot}6H_2O$ and NEt_3 in different solvents resulted in the formation of crystalline $[(cool)\{Co^{II}(\mu\text{-}OH)Co^{II}\}](ClO_4)_3$. Single-crystals provided single-crystal X-ray diffraction data, that were not of sufficient quality to allow a satisfactory refinement. Using $Co(OTf)_2{\cdot}7H_2O$ and subsequent addition of $NaBPh_4$ provided single-crystals of sufficient quality for single-crystal X-ray diffraction and analyzed as $[(cool)\{Co^{II}(\mu\text{-}OH)Co^{II}\}](BPh_4)_2(OTf){\cdot}2CH_3CN$. For the synthesis of complexes of cool with exogenous halide ligands, the synthetic strategy of the analogue susan complexes was adapted.[16] The reaction of cool with a 1 : 1 mixture of $CoCl_2{\cdot}6H_2O$/$Co(ClO_4)_2{\cdot}6H_2O$ in MeOH/EtOH provided the complex $[(cool)\{Co^{II}Cl\}_2](ClO_4)_2$, using $CoBr_2$ instead of $CoCl_2{\cdot}6H_2O$ provided $[(cool)\{Co^{II}Br\}_2](ClO_4)_2$.

In analogy, the reaction of $susan^{OMe}$ with a 1 : 1 mixture of $CoCl_2{\cdot}6H_2O$/$Co(ClO_4)_2{\cdot}6H_2O$ or $CoBr_2$/$Co(ClO_4)_2{\cdot}6H_2O$ in MeOH/EtOH provided $[(susan^{OMe})\{Co^{II}Cl\}_2](ClO_4)_2$ or $[(susan^{OMe})\{Co^{II}Br\}_2](ClO_4)_2$, respectively. The reaction of $susan^{OMe}$ with $Co(ClO_4)_2{\cdot}6H_2O$ and NEt_3 under a N_2-blanketing atmosphere provided the μ-hydroxo bridged complex $[(susan^{OMe})\{Co^{II}(\mu\text{-}OH)Co^{II}\}](ClO_4)_3$. Attempts to obtain a CH_3CN complex with the ligand $susan^{OMe}$ provided only oils. The reaction of $susan^{6\text{-}Me}$ and $Co(ClO_4)_2{\cdot}6H_2O$ in CH_3CN provided the complex $[(susan^{6\text{-}Me})\{Co^{II}(CH_3CN)_2\}_2](ClO_4)_4$. The bis-μ-hydroxo bridged complex $[(susan^{6\text{-}Me})\{Co^{II}(\mu\text{-}OH)_2Co^{II}\}](ClO_4)_2$ was obtained from the reaction of $susan^{6\text{-}Me}$ with $Co(ClO_4)_2{\cdot}6H_2O$ and NEt_3 in MeOH.

Structural characterization

All new complexes were characterized by single-crystal X-ray diffraction. Details of the crystal structures are provided in the Experimental section. Instead of describing the individual molecular structures, the differences between the molecular structures of the nine complexes described herein and of the already published susan complexes will be analyzed to determine the influence of the dinucleating and the exogenous ligands. The molecular structures of the complex cations are shown in Fig. 1, thermal ellipsoid plots in Fig. S4,† and selected interatomic distances are given in Table 1. Mean bond lengths with two decimal places are provided in Table 2 to avoid on the one hand chemically not-relevant differences and on the other hand the inclusion of standard deviations for the comparison.

One obvious difference is the coordination number of the CH_3CN complexes. Six-coordinate Co^{II} ions were obtained with the ligands susan and $susan^{6\text{-}Me}$ having two CH_3CN ligands per Co^{II}, while the ligand cool provides five-coordinate Co^{II} ions with one CH_3CN ligand. This difference cannot be attributed to sterical effects as the imidazole donors of cool are sterically the least demanding. Hence, this five-coordination demonstrates the higher electron donation capability of cool than of susan and $susan^{6\text{-}Me}$.

The two closely related complexes $[(susan)\{Co^{II}(CH_3CN)_2\}_2]^{4+}$ and $[(susan^{6\text{-}Me})\{Co^{II}(CH_3CN)_2\}_2]^{4+}$ nicely demonstrate the effect of the introduction of the 6-Me substituents on the pyridine donors. The N_3-subunit diphenylamine (DPA) of the ligand susan coordinates meridionally but that of the ligand $susan^{6\text{-}Me}$ coordinates facially. If the ligand $susan^{6\text{-}Me}$ coordinated also meridionally, both 6-Me groups would directly point to one CH_3CN. This is avoided by the facial coordination of $susan^{6\text{-}Me}$ preventing this steric hinderance with one CH_3CN ligand. However, the sterical repulsion of the two 6-Me group with the CH_3CN ligand (N6) is still effective resulting in longer mean Co–$N^{6\text{-}Me\text{-}py}$ bonds (2.20 Å) than the mean Co–N^{py} bonds

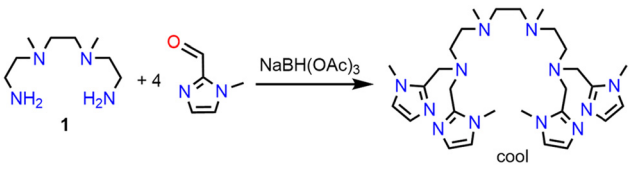

Scheme 2 Synthesis of the ligand cool.

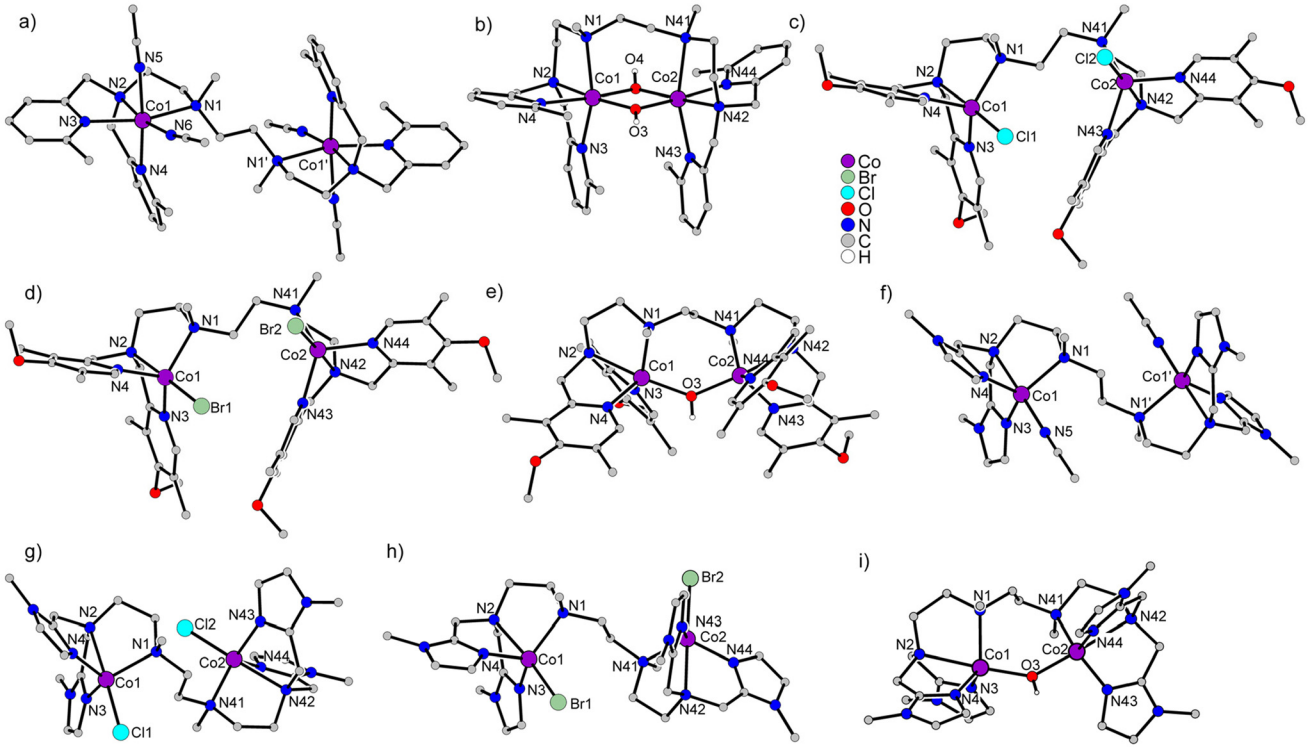

Fig. 1 Molecular structures of (a) $[(susan^{6\text{-}Me})\{Co^{II}(CH_3CN)_2\}_2]^{4+}$ in single-crystals of $[(susan^{6\text{-}Me})\{Co^{II}(CH_3CN)_2\}_2](ClO_4)_4$, (b) $[(susan^{6\text{-}Me})\{Co^{II}(\mu\text{-}OH)_2Co^{II}\}]^{2+}$ in single-crystals of $[(susan^{6\text{-}Me})\{Co^{II}(\mu\text{-}OH)_2Co^{II}\}](ClO_4)_2\cdot MeOH$, (c) $[(susan^{OMe})\{Co^{II}Cl\}_2]^{2+}$ in single-crystals of $[(susan^{OMe})\{Co^{II}Cl\}_2](ClO_4)_2\cdot 3MeOH$, (d) $[(susan^{OMe})\{Co^{II}Br\}_2]^{2+}$ in single-crystals of $[(susan^{OMe})\{Co^{II}Br\}_2](ClO_4)_2\cdot 3MeOH$, (e) $[(susan^{OMe})Co^{II}(\mu\text{-}OH)Co^{II}]^{3+}$ in single-crystals of $[(susan^{OMe})Co^{II}(\mu\text{-}OH)Co^{II}](ClO_4)_3\cdot 3CH_3CN$, (f) $[(cool)\{Co^{II}(CH_3CN)\}_2]^{4+}$ in single-crystals of $[(cool)\{Co^{II}(CH_3CN)\}_2](ClO_4)_4\cdot 2CH_3CN$, (g) $[(cool)\{Co^{II}Cl\}_2]^{2+}$ in single-crystals of $[(cool)\{Co^{II}Cl\}_2](ClO_4)_2$, (h) $[(cool)\{Co^{II}Br\}_2]^{2+}$ in single-crystals of $[(cool)\{Co^{II}Br\}_2](ClO_4)_2$, and (i) $[(cool)Co^{II}(\mu\text{-}OH)Co^{II}]^{3+}$ in single-crystals of $[(cool)Co^{II}(\mu\text{-}OH)Co^{II}](BPh_4)_2(CF_3SO_3)\cdot 2CH_3CN$. Hydrogen atoms, counter ions and solvent molecules are omitted for clarity.

(2.10 Å). This different coordination of the ligands susan and $susan^{6\text{-}Me}$ also influences the Co–N^{am} distances, which are Co1–N1 = 2.22 Å and Co1–N2 = 2.15 Å with susan, where both amine donors coordinate *trans* to a CH_3CN donor. In contrast, with $susan^{6\text{-}Me}$, Co1–N1 *trans* to a pyridine elongates to 2.32 Å, while Co1–N2 *trans* to a CH_3CN decreases to 2.10 Å.

In $[(cool)\{Co^{II}(CH_3CN)\}_2]^{4+}$, the mean Co–$N^{im}$ bond lenghts are shorter at 2.00 Å indicating a stronger electron donation ability of the imidazoles. However, a direct comparison between five- and six-coordinate complexes can be misleading as a lower-coordinate metal ion requires more electron donation and therefore shorter bond lengths for similar donor types.

In the chloride and bromide complexes of cool, $susan^{OMe}$, and susan, the Co^{II} ions are all five-coordinate close to trigonal–bipyramidal ($\tau \sim 0.9$) allowing a direct comparison of the aromatic nitrogen donors. In $[(cool)\{Co^{II}Cl\}_2]^{2+}$ and $[(cool)\{Co^{II}Br\}_2]^{2+}$, the Co–$N^{im}$ bonds are 2.01 Å, while the Co–N^{py} bonds are 2.06 Å in $[(susan^{OMe})\{Co^{II}Cl\}_2]^{2+}$, $[(susan^{OMe})\{Co^{II}Br\}_2]^{2+}$, $[(susan)\{Co^{II}Cl\}_2]^{2+}$, and $[(susan)\{Co^{II}Br\}_2]^{2+}$ demonstrating stronger bonds with an imidazole donor compared to a pyridine donor. This indicates besides minor π-bonding effects mainly a stronger σ-donor interaction of the imidazole donors. The shorter Co–N^{im} bonds result in longer Co–N2 bonds of the amine in *cis* position (2.32–2.33 Å) compared to 2.17–2.23 Å with the pyridine donors.

For all four ligands, μ-hydroxo-bridged complexes were obtained under basic conditions. While the Co^{II} ions in the complexes with the ligands susan, $susan^{OMe}$, and cool are five-coordinate with only one μ-hydroxo-bridge, the Co^{II} ions in the complex with the ligand $susan^{6\text{-}Me}$ are six-coordinate with two μ-hydroxo-bridges. This difference nicely demonstrates the lower electron donation of the ligand $susan^{6\text{-}Me}$ due to the longer Co^{II}–$N^{6\text{-}Me\text{-}py}$ bonds leading to a coordinatively unsaturated situation for only one μ-hydroxo-bridge. The resulting "diamond-core" in $[(susan^{6\text{-}Me})\{Co^{II}(\mu\text{-}OH)_2Co^{II}\}]^{2+}$ shows alternating short 1.96 and long 2.13 Å Co–O(H) bonds, which was also observed for corresponding diferrous complexes.[26]

In the five-coordinate μ-hydroxy-bridged complexes the same trend as in the five-coordinate halide complexes is observed. The Co–N^{im} bond lengths are 2.02 Å while the Co–N^{py} are longer in $[(susan^{OMe})Co^{II}(\mu\text{-}OH)Co^{II}]^{3+}$ (2.06/2.07 Å) and in $[(susan)Co^{II}(\mu\text{-}OH)Co^{II}]^{3+}$ (2.08 Å). Interestingly, this difference has no significant influence on the Co-μ-OH bond lengths, which are all in the range 1.96–1.97 Å. However, the other apical donor of the trigonal bipyramide (N2) is significantly elongated 2.30 Å with cool compared to 2.20 Å with

Table 1 Selected interatomic distances (Å) and angles (°)

		[(susan$^{6\text{-Me}}$){Co(μ-OH)$_2$Co}](ClO$_4$)$_2$·MeOH		[(susan^{OMe}){CoCl}$_2$](ClO$_4$)$_2$·3MeOH		[(susan^{OMe}){CoBr}$_2$](ClO$_4$)$_2$·3MeOH		[(susan^{OMe})Co(μ-OH)Co](ClO$_4$)$_3$·3CH$_3$CN	
	[(susan$^{6\text{-Me}}$){Co(CH$_3$CN)$_2$}$_2$](ClO$_4$)$_4$	Co1-side	Co2-side[a]	Co1-side	Co2-side[a]	Co1-side	Co2-side[a]	Co1-side	Co2-side[a]
Co1–N1	2.3175(14)	2.327(2)	2.403(2)	2.135(2)	2.112(2)	2.1381(18)	2.1265(19)	2.1398(14)	2.1456(15)
Co1–N2	2.1028(14)	2.148(2)	2.141(2)	2.172(2)	2.1736(19)	2.177(2)	2.1688(17)	2.1952(15)	2.1998(16)
Co1–N3	2.1950(14)	2.220(2)	2.225(2)	2.070(2)	2.051(2)	2.068(2)	2.0580(17)	2.0739(14)	2.0595(15)
Co1–N4	2.1918(14)	2.261(2)	2.236(2)	2.064(2)	2.046(2)	2.069(2)	2.0488(19)	2.0419(15)	2.0731(15)
Co1–X[b]	2.1984(15)	1.9557(19)	2.105(2)	2.2763(7)	2.3050(7)	2.4186(4)	2.4486(3)	1.9756(13)	1.9694(13)
Co1–Y[b]	2.0718(15)	2.1530(19)	1.9540(19)						
Co1···Co2[c]	7.8707(6)	3.1763(6)		5.7559(5)		5.7568(4)		3.6616(5)	
N1–Co1–N2	81.56(5)	80.83(8)	79.47(9)	82.28(8)	81.55(8)	82.37(7)	81.55(7)	81.11(5)	81.70(6)
N1–Co1–N3	159.65(5)	156.58(8)	155.98(8)	124.38(8)	125.93(8)	123.82(7)	127.23(7)	130.46(6)	103.60(6)
N1–Co1–N4	87.42(5)	83.23(8)	81.94(8)	108.59(8)	111.80(8)	110.15(7)	109.97(7)	106.20(6)	131.58(6)
N1–Co1–X[b]	93.27(5)	99.86(8)	93.13(8)	100.25(6)	97.61(6)	99.23(5)	97.94(5)	97.33(6)	97.79(6)
N1–Co1–Y	91.15(6)	94.60(7)	95.62(8)						
N2–Co1–N3	78.58(6)	75.76(8)	76.61(9)	77.82(9)	77.54(7)	77.71(9)	77.42(6)	76.59(6)	78.32(6)
N2–Co1–N4	82.72(5)	79.31(8)	80.80(9)	77.99(8)	78.32(8)	78.26(8)	78.11(7)	78.82(6)	76.08(6)
N2–Co1–X[b]	90.25(6)	167.69(8)	93.58(8)	177.36(6)	178.09(6)	178.05(5)	177.45(5)	172.89(5)	173.37(6)
N2–Co1–Y[b]	169.97(6)	90.37(8)	170.53(9)						
N3–Co1–N4	94.37(5)	91.96(8)	92.07(8)	116.91(8)	111.80(8)	116.10(8)	112.07(7)	111.89(6)	112.99(6)
N3–Co1–X[b]	82.49(5)	103.10(8)	90.52(8)	101.19(7)	101.67(6)	102.20(6)	101.02(5)	99.53(6)	108.16(6)
N3–Co1–Y[b]	107.99(6)	86.04(7)	108.37(8)						
N4–Co1–X[b]	172.76(5)	112.99(8)	173.08(8)	100.41(6)	103.59(6)	100.10(5)	104.39(5)	108.24(6)	99.66(6)
N4–Co1–Y[b]	103.93(6)	169.67(8)	106.69(8)						
X[b]–Co1–Y[b]	83.27(6)	77.32(8)	78.52(8)						
Co1–O3–Co2		102.87(9)						136.30(7)	
Co1–O4–Co2		101.21(8)							

		[(cool){CoCl}$_2$](ClO$_4$)$_2$		[(cool){CoBr}$_2$](ClO$_4$)$_2$		[(cool)Co(μ-OH)Co](BPh$_4$)$_2$(CF$_3$SO$_3$)·2CH$_3$CN	
	[(cool){Co(CH$_3$CN)}$_2$](ClO$_4$)$_4$·2CH$_3$CN	Co1-side	Co2-side[a]	Co1-side	Co2-side[a]	Co1-side	Co2-side[a]
Co1–N1	2.093(2)	2.116(3)	2.107(3)	2.1097(16)	2.1145(16)	2.1488(11)	2.1411(11)
Co1–N2	2.273(2)	2.320(3)	2.342(2)	2.3327(16)	2.3069(17)	2.3407(11)	2.3820(11)
Co1–N3	1.998(2)	2.016(3)	2.013(3)	2.0080(17)	2.0107(16)	2.0263(11)	1.9924(12)
Co1–N4	2.001(2)	2.024(3)	2.000(3)	2.0015(17)	2.0198(17)	2.0210(12)	2.0148(11)
Co1–X[d]	2.052(2)	2.3015(9)	2.2898(9)	2.4421(3)	2.4471(3)	1.9586(10)	1.9769(10)
Co1···Co2[e]	6.1573(19)	5.8531(9)		5.9247(4)		3.6323(2)	
N1–Co1–N2	81.89(8)	80.43(10)	80.06(9)	80.50(6)	80.95(6)	79.67(4)	80.08(4)
N1–Co1–N3	121.59(9)	119.72(10)	122.02(10)	122.00(6)	119.66(7)	122.73(4)	110.24(5)
N1–Co1–N4	110.51(9)	107.58(11)	116.48(11)	115.00(7)	108.75(7)	109.04(5)	118.01(5)
N1–Co1–X[d]	98.87(9)	101.76(8)	102.76(8)	104.83(5)	101.69(5)	98.32(4)	101.42(4)
N1–Co1–Y							
N2–Co1–N3	78.53(8)	75.60(10)	76.83(9)	76.82(6)	75.87(6)	76.11(4)	77.18(4)
N2–Co1–N4	78.88(8)	76.61(11)	77.11(10)	77.03(6)	76.84(7)	77.75(4)	76.08(4)
N2–Co1–X[d]	177.82(9)	176.78(7)	176.09(7)	173.93(4)	176.76(4)	175.98(4)	175.43(4)
N2–Co1–Y[d]							
N3–Co1–N4	118.54(9)	118.86(11)	108.91(11)	110.66(7)	118.50(7)	115.10(4)	118.51(5)
N3–Co1–X[d]	102.71(9)	101.22(8)	103.63(8)	102.29(5)	101.11(5)	102.31(4)	106.13(4)
N3–Co1–Y[d]							
N4–Co1–X[d]	98.94(9)	104.79(8)	99.13(8)	97.85(5)	103.89(5)	106.24(4)	99.46(4)
N4–Co1–Y[d]							
X[d]–Co1–Y[d]							
Co1–O3–Co2						134.73(6)	
Co1–O4–Co2							

[a] The numbering scheme of the Co2 side or molecule has been adapted according to the Co1 side. [b] X = Br, Cl, CH$_3$CN, or μ-OH; Y = CH$_3$CN, or μ-OH. [c] Intramolecular Co···Co distance and angle, which is Co1···Co1′ with $-x$, $1-y$, $2-z$ for [(susan$^{6\text{-Me}}$){Co^{II}(CH$_3$CN)$_2$}$_2$](ClO$_4$)$_4$. [d] X = Br, Cl, MeCN, or μ-OH. [e] Intramolecular Co···Co distance and angle, which is Co1···Co1′ with $2-X$, $1-Y$, $1-Z$ for [(cool)Co^{II}(μ-OH)Co^{II}](BPh$_4$)$_2$(CF$_3$SO$_3$)·2CH$_3$CN.

Table 2 Selected interatomic mean distances (Å), τ values,[29] spin-Hamiltonian parameters, and electrochemical data for the complexes [(L){$Co^{II}(XY)$}$_2$]$^{n+}$ (L = susan,[16] susan$^{6\text{-Me}}$, susan^{OMe}, and cool)

	Co–N1	Co–N2	Co–N3	Co–N4	Co–X	Co–Y	τ	J/cm^{-1}	g	D/cm^{-1}	E^p/V *vs.* Fc$^+$/Fc[a]	
X(=Y)=CH$_3$CN												
susan	2.22	2.15	2.09	2.10	2.24	2.08		−0.41	2.43	40.9	0.91, 0.46	−1.53, *−1.9*
susan$^{6\text{-Me}}$	2.32	2.10	2.20	2.19	2.20	2.07		−0.33	2.55	68.5	1.49	−1.41, *−1.9*
cool	2.09	2.27	1.99	2.00	2.05		0.94	−1.2	2.19	10	1.47	−1.76, −2.4
X = Cl												
susan	2.12	2.23	2.05	2.07	2.29		0.88/0.91	−0.68	2.25	6.9	1.08	−1.91, −2.1
susan^{OMe}	2.12	2.17	2.06	2.05	2.29		0.88/0.87	−0.01	2.29	6.1	1.10	−2.1
cool	2.11	2.33	2.01	2.01	2.30		0.95/0.90	−0.24	2.24	3.2	1.02	−2.4
X = Br												
susan	2.13	2.19	2.06	2.06	2.44		0.91/0.86	−0.12	2.25	5.8	0.75	−1.83, −1.9
susan^{OMe}	2.13	2.17	2.06	2.06	2.43		0.90/0.87	−0.10	2.33	6.0	0.79	−2.03, −2.1
cool	2.11	2.32	2.01	2.01	2.44		0.87/0.95	−0.29	2.25	4.2	0.77	−2.4
X(=Y)=OH												
susan	2.17	2.20	2.08	2.08	1.96		0.74/0.75	−18.8	2.29	D_1 = 65/D_2 = 17	1.31	−1.9
susan$^{6\text{-Me}}$	2.37	2.14	2.22	2.25	1.96	2.13		+2.4	2.46/2.50	D_1 = −56/D_2 = −16	1.26, 0.72	
susan^{OMe}	2.14	2.20	2.07	2.06	1.97		0.71/0.70	−20.8	2.29	D_1 = 56/D_2 = 8	1.24	−2.1
cool	2.15	2.36	2.01	2.02	1.97		0.89/0.95	−14.5	2.18	86.4	1.18	−2.4

[a] Values in italics are $E^{\circ\prime}$ for reversible redox waves.

susan and susan^{OMe} as already observed in the halide complexes.

In summary, the differences in the structural parameters allow to conclude, that the electron-density donation ability is in the order susan$^{6\text{-Me}}$ < susan/susan^{OMe} < cool. No significant structural differences are observed for complexes of the ligands susan^{OMe} and susan allowing no differentiation of their electron-donation ability.

Magnetic properties

To investigate the magnetic properties of the dinuclear Co^{II} complexes, the temperature-dependence of the effective magnetic moments, μ_{eff}, (Fig. 2) and the variable-temperature variable-field VTVH magnetization (Fig. 3) were measured. These magnetic data were analyzed on the basis of the usual spin-Hamiltonian description for the electronic ground state for exchange coupled systems.[27] The spin-Hamiltonian employed was:

$$\hat{H} = -2J\hat{S}_1\hat{S}_2 + \sum_{i=1}^{2} D_i \hat{S}_{z,i}{}^2 + \sum_{i=1}^{2} g_i \mu_B \hat{S}_i B \qquad (1)$$

where the first term is the isotropic Heisenberg-Dirac-van Vleck (HDvV) exchange operator with J is the exchange coupling constant, the second term the axial zero-field splitting operator under the condition of co-axial zero-field splitting tensors with D_i the axial zero-field splitting parameter, and the third term the Zeeman operator with g_i the average electronic g value. Magnetic moments were obtained from numerically generated derivatives of the eigenvalues of eqn (1) and summed up over 16 field orientations along a 16-point Lebedev grid to account for the powder distribution of the sample. The limitations of the applicability of this spin-Hamiltonian and the applied fitting procedure are described in our previous study.[16] For each complex, the μ_{eff} *vs.* T and VTVH data were fitted simultaneously with one parameter set.

The complex [(susan$^{6\text{-Me}}$){$Co^{II}(CH_3CN)_2$}$_2$](ClO$_4$)$_4$ exhibits μ_{eff} = 6.92μ_B at 300 K that decreases by decreasing temperature with a stronger decrease below 100 K reaching 4.02μ_B at 2 K (Fig. 2a). The VTVH data exhibit a slight nesting behavior of the iso-field lines (Fig. 3a). Fitting these data provided a small coupling constant J = −0.33 cm^{-1}, a large deviation from g_e = 2.00 with g = 2.55, and a large value of D = 68.5 cm^{-1}. The μ_{eff} of 6.87μ_B at 300 K of [(susan$^{6\text{-Me}}$){Co^{II}(μ-OH)$_2$$Co^{II}$}](ClO$_4$)$_2$ increases by decreasing the temperature, reaches a maximum of 7.45μ_B at 11 K, and drops to a value of 5.48μ_B at 2 K (Fig. 2a). This behavior indicates a ferromagnetic coupling between the Co^{II} ions. This sample was measured in eicosane to prevent potential torquing effects in high magnetic fields. The VTVH data (Fig. 3b) show a slight nesting behavior of the iso-field lines. Fitting these data provided the ferromagnetic coupling constant J = 2.4 cm^{-1}, g values of g_1 = 2.46 and g_2 = 2.50, and zero-field splittings of D_1 = −56 cm^{-1} and D_2 = −16 cm^{-1}. Corresponding differences for the two Co^{II} ions have already been observed for [(susan){Co^{II}(μ-OH)Co^{II}}](ClO$_4$)$_3$ (Table 2).[16]

The halide complexes [(susan^{OMe}){$Co^{II}Cl$}$_2$](ClO$_4$)$_2$·3MeOH and [(susan^{OMe}){$Co^{II}Br$}$_2$](ClO$_4$)$_2$ exhibit almost the same temperature-dependence of μ_{eff} (Fig. 2b). The value of μ_{eff} for [(susan^{OMe}){$Co^{II}Cl$}$_2$](ClO$_4$)$_2$·3MeOH is 6.29μ_B at 300 K and shows a decrease below 30 K to a value of 4.85μ_B at 2 K. For [(susan^{OMe}){$Co^{II}Br$}$_2$](ClO$_4$)$_2$·3MeOH, μ_{eff} is 6.38μ_B at 300 K and drops to 4.79μ_B at 2 K. In combination with the VTVH (Fig. 3c + d), the following parameter sets were obtained: X = Cl: g = 2.29, J = −0.01 cm^{-1}, D = 6.1 cm^{-1}; X = Br: g = 2.33, J = −0.10 cm^{-1} and D = 6.0 cm^{-1}.

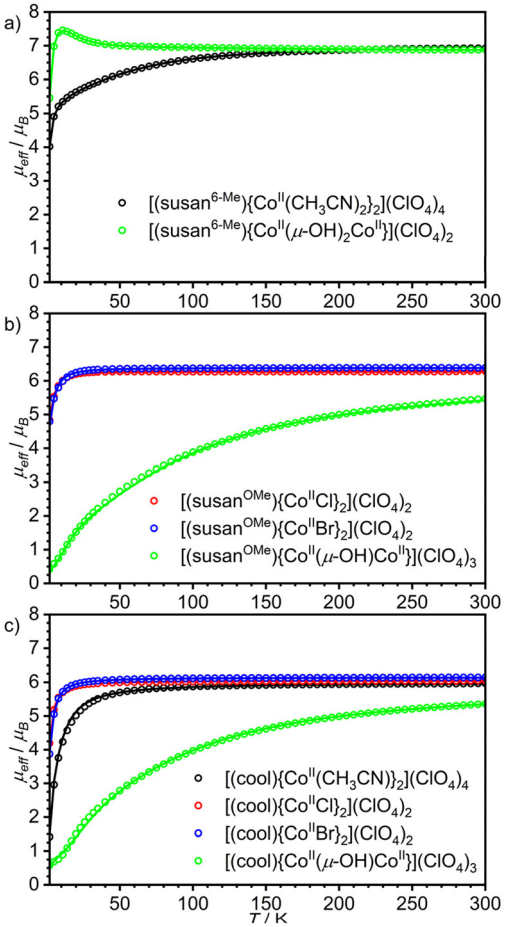

Fig. 2 Temperature dependence of the effective magnetic moment, μ_{eff}, for the dinuclear $Co^{II}Co^{II}$ complexes of the ligands (a) susan$^{6\text{-Me}}$, (b) susan^{OMe}, and (c) cool. Open circles correspond to the experimental data and solid lines correspond to simulations using the spin-Hamiltonian provided in eqn (1) and parameters provided in Table 2. The sample of [(susan$^{6\text{-Me}}$){Co^{II}(μ-OH)$_2$Co^{II}}](ClO$_4$)$_2$ was measured in eicosane.

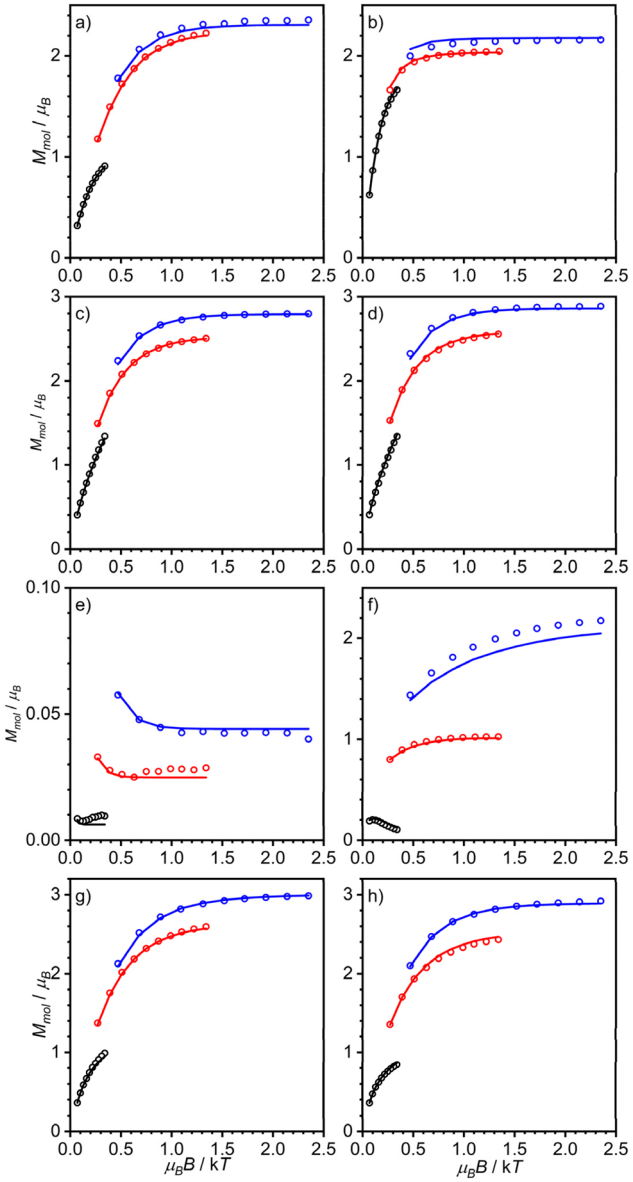

Fig. 3 Variable-temperature variable-field magnetization data of (a) [(susan$^{6\text{-Me}}$){Co^{II}(CH$_3$CN)$_2$}$_2$](ClO$_4$)$_4$·H$_2$O, (b) [(susan$^{6\text{-Me}}$){Co^{II}(μ-OH)$_2$Co^{II}}](ClO$_4$)$_2$·1.5H$_2$O (measured in eicosane), (c) [(susan^{OMe}){Co^{II}Cl}$_2$](ClO$_4$)$_2$·3MeOH, (d) [(susan^{OMe}){Co^{II}Br}$_2$](ClO$_4$)$_2$·3MeOH, (e) [(susan^{OMe})Co^{II}(μ-OH)Co^{II}](ClO$_4$)$_3$·1.5H$_2$O, (f) [(cool){Co^{II}(CH$_3$CN)}$_2$](ClO$_4$)$_4$·CH$_3$CN, (g) [(cool){Co^{II}Cl}$_2$](ClO$_4$)$_2$·MeOH, and (h) [(cool){Co^{II}Br}$_2$](ClO$_4$)$_2$·MeOH. Open circles correspond to the experimental data and solid lines correspond to simulations using the spin-Hamiltonian provided in eqn (1) and parameters provided in Table 2.

The complex [(susan^{OMe}){Co^{II}(μ-OH)Co^{II}}](ClO$_4$)$_3$ exhibits a similar coordination environment for the two Co^{II} ions as in the halide complexes but μ_{eff} = 5.47μ_B at 300 K steadily decreases with decreasing temperature to 0.42μ_B at 2 K (Fig. 2b). This comparison clearly demonstrates that besides the local magnetic anisotropies, a considerable antiferromagnetic exchange is mediated by the bridging hydroxo ligand. This behavior closely resembles that of the complex [(susan){Co^{II}(μ-OH)Co^{II}}](ClO$_4$)$_3$ (Table 2)[16] and fitting provided J = −20.8 cm^{-1}, g = 2.29, D_1 = 56 cm^{-1}, and D_2 = 8 cm^{-1}.

The three non-bridged complexes of the ligand cool [(cool){Co^{II}(CH$_3$CN)}$_2$](ClO$_4$)$_4$, [(cool){Co^{II}Cl}$_2$](ClO$_4$)$_2$, and [(cool){Co^{II}Br}$_2$](ClO$_4$)$_2$ show μ_{eff} of 5.96, 6.04, and 6.15μ_B at 300 K, respectively (Fig. 2c), that decrease below 50 K to 4.19μ_B for [(cool){Co^{II}Cl}$_2$](ClO$_4$)$_2$ and 3.87μ_B for [(cool){Co^{II}Br}$_2$](ClO$_4$)$_2$ at 2 K. The complex [(cool){Co^{II}(CH$_3$CN)}$_2$](ClO$_4$)$_4$ exhibits a slightly stronger decrease of μ_{eff} below ~100 K reaching a lower value of 1.42μ_B at 2 K. This can be rationalized by π–π-interactions between two neighboring molecules observed in the crystal-structure (Fig. S6†), that lead to a stronger antiferromagnetic exchange. Fitting these data provided the following parameter sets: X = CH$_3$CN: J = −1.2 cm^{-1}, g = 2.19, D = 10.0 cm^{-1}; X = Cl: J = −0.24 cm^{-1}, g = 2.21, D = 3.2 cm^{-1}; X = Br: J = −0.29 cm^{-1}, g = 2.25, D = 4.2 cm^{-1}. The occurrence of the bridging hydroxo ligand in [(cool){Co^{II}(μ-OH)Co^{II}}](BPh$_4$)$_2$(OTf) coincides again with a stronger temperature-dependence from 5.36μ_B at 300 K to 0.58μ_B at 2 K (Fig. 2c). The fitting provided J = −15.5 cm^{-1}, g = 2.18, and D = 86.4. The

VTVH data were not considered as they provided no contribution of the complex due to the almost not existing magnetization at low temperature.

The magnetic properties reflect the electronic structures of the complexes that are governed for these $Co^{II}Co^{II}$ complexes by their molecular structures. An important aspect is the deviation of the coordination polyhedra from an ideal octahedron. In the latter, the $^4T_{1g}$ ground state has a first-order orbital angular momentum. The larger the distortion from octahedral symmetry, the stronger is the splitting of the $^4T_{1g}$ reducing the orbital angular momentum contribution. When the splitting is large enough, the remaining orbital angular momentum can be treated by second order spin–orbit coupling and phenomenologically by zero-field splitting in the spin-Hamiltonian description. This is manifested here by zero-field splittings $|D|$ in the order of 40–70 cm^{-1} for six-coordinate complexes and <10 cm^{-1} for the five-coordinate complexes with exogenous halide ligands. For the μ-hydroxo-bridged complexes, a smaller and a larger $|D|$ is found also for the five-coordinate complexes; a situation already found for the susan complexes.[16] In summary, as the electron-donating abilities of the exogenous and dinucleating ligands determine the coordination number, the magnetic properties reflect these differences and again no differentiation can be made between susan and susan^{OMe}.

Electronic absorption spectroscopy

The electronic absorption spectra of the complexes and ligands in CH_3CN are shown in Fig. 4. The ligands susan$^{6\text{-}Me}$ (ref. 19) and susan^{OMe} (ref. 13) exhibit intense absorptions at 37 600 cm^{-1} ($\varepsilon = 16.4 \times 10^3$ M^{-1} cm^{-1}) and 38 000 cm^{-1} ($\varepsilon = 9.9 \times 10^3$ M^{-1} cm^{-1}), respectively, that can be assigned to π–π* transitions of the pyridines. The dinuclear $Co^{II}Co^{II}$ complexes of these ligands exhibit similar bands that exhibit therefore strong ligand π–π* character. The imidazoles in the ligand cool exhibit no such band in this energy region, so that absorptions of the dinuclear $Co^{II}Co^{II}$ complexes in this energy region can be attributed to have contributions from the Co^{II} ions.

The $Co^{II}Co^{II}$ complexes show multiple absorptions in the range 5000–25 000 cm^{-1} (Fig. 4 insets) that mainly arise from d–d transitions and unspecific more intense absorptions at higher energies that are mainly charge-transfer in nature. The spectra of the $Co^{II}Co^{II}$ complexes of the ligand susan[16] closely resemble those of the ligand susan^{OMe} having the same exogenous donors. We presented a detailed assignment and analysis of the d–d transitions of the susan $Co^{II}Co^{II}$ complexes[16] and therefore refrain from repeating this here. Instead, we focus on specific signatures that may allow to deduce molecular structures in solution.

Generally, energies and molar extinction coefficients differ significantly for five- and six-coordinated complexes. The six-coordinate complexes show a weak band around 9000 cm^{-1} ($[(susan^{6\text{-}Me})\{Co^{II}(CH_3CN)_2\}_2]^{4+}$ 8700 cm^{-1}, ε = 14 M^{-1} cm^{-1}; $[(susan^{6\text{-}Me})\{Co^{II}(\mu\text{-}OH)_2Co^{II}\}]^{2+}$ 8800 cm^{-1}, ε = 9 M^{-1} cm^{-1}) and not well-resolved transitions in the range 17 000–23 000 cm^{-1} with ε below 100 M^{-1} cm^{-1}. The same signature was observed for $[(susan)\{Co^{II}(CH_3CN)_2\}_2]^{4+}$ while

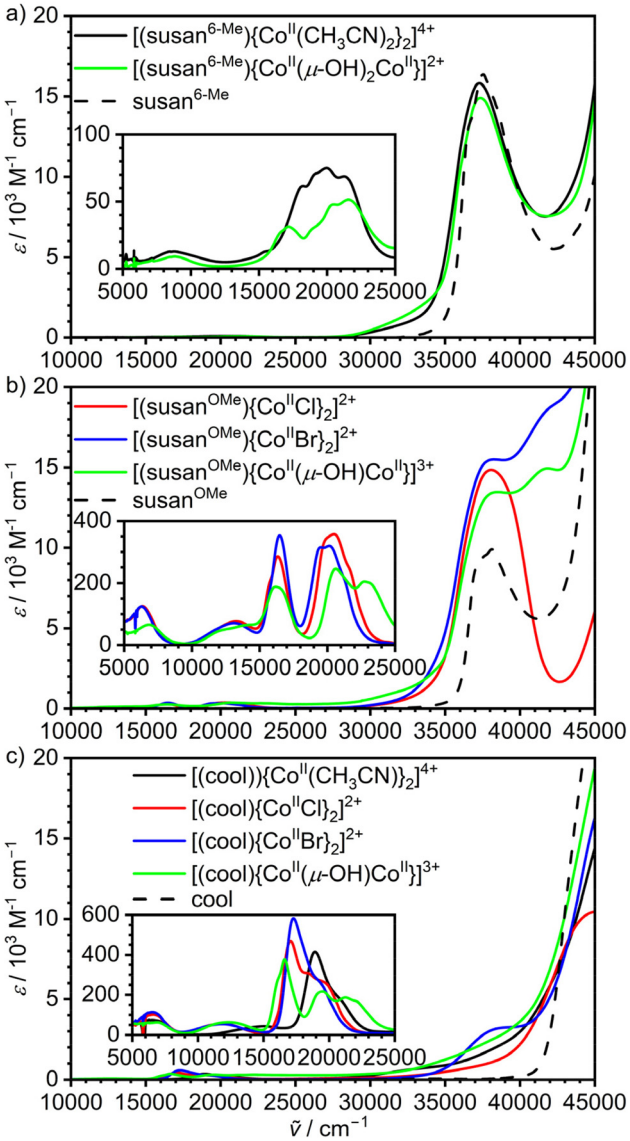

Fig. 4 UV-Vis-NIR spectra of the dinuclear Co^{II}_2 complexes of the ligands (a) susan$^{6\text{-}Me}$, (b) susan^{OMe}, and (c) cool. and the different ligands dissolved in CH_3CN.[13,19]

$[(susan)Co^{II}(\mu\text{-}OH)Co^{II}]^{3+}$ resembles the spectra of the five-coordinate complexes.[16] This shows that not only $[(susan^{6\text{-}Me})\{Co^{II}(CH_3CN)_2\}_2]^{4+}$ and $[(susan)\{Co^{II}(CH_3CN)_2\}_2]^{4+}$ but also $[(susan^{6\text{-}Me})\{Co^{II}(\mu\text{-}OH)_2Co^{II}\}]^{2+}$ remains six-coordinate in solution and that the two hydroxo-bridged complexes $[(susan^{6\text{-}Me})\{Co^{II}(\mu\text{-}OH)_2Co^{II}\}]^{2+}$ and $[(susan)Co^{II}(\mu\text{-}OH)Co^{II}]^{3+}$ can be easily differentiated in solution by their UV-Vis spectra.

The five-coordinate complexes all exhibit a d–d transition below 7000 cm^{-1} of higher intensity (ε > 50 M^{-1} cm^{-1}). At higher energies, a well-resolved transition around 16 500–17 500 cm^{-1} is characteristic besides a band around 20 000 cm^{-1}. The three $\mu\text{-}OH^-$ bridged $Co^{II}Co^{II}$ complexes of susan, susan^{OMe}, and cool exhibit a further distinct band around 22 000–23 000 cm^{-1}. Hence, this feature is characteristic for the $\{Co^{II}(\mu\text{-}OH)Co^{II}\}$ core of the five-coordinate $Co^{II}Co^{II}$

complexes and can – in other words – serve to assign the persistence of the μ-OH^- bridge in solution.

The spectra of the $Co^{II}Co^{II}$ complexes of $susan^{OMe}$ (Fig. 4b) show no strong differences with those of susan having the same exogenous donor, but differ significantly from those of cool (Fig. 4c) in the 15 000–25 000 cm^{-1} region. The distinct bands below 19 000 cm^{-1} are of lower intensity in the spectra of the $susan^{OMe}$ complexes (ε < 370 M^{-1} cm^{-1}) than of the cool complexes (ε > 370 M^{-1} cm^{-1}). Moreover, this band does not significantly shift for the $susan^{OMe}$ complexes (16 200–16 500 cm^{-1}), while a significant shift is observed for the cool complexes (μ-OH^-: 16 600 cm^{-1}, Cl^-: 17 100 cm^{-1}, 17 300 cm^{-1}). These absorptions were assigned to $^4A'_2 \rightarrow {}^4A'_2$ (^4P) transitions, which do not involve significant $d(z^2)$ character and are therefore not strongly sensitive to the nature of the axial donors in trigonal-bipyramidally coordinated Co^{II} ions.[16] Hence, the change of π-acceptor ligands pyridine with π-donor ligands imidazole influence these transitions. A further observation is that the well-resolved transitions around 20 000 cm^{-1} in the $susan^{OMe}$ complexes decrease in intensity and become less well-resolved in the cool complexes.

A special effect is observed for $[(cool)\{Co^{II}(CH_3CN)\}_2]^{4+}$ – the only five-coordinate complex with an axial CH_3CN donor. The other $Co^{II}Co^{II}$ complexes of cool exhibit one band around 12 100 cm^{-1} and the characteristic absorptions between 16 600–17 300 cm^{-1}. These bands shift to 15 100 and 18 900 cm^{-1}, respectively, for $[(cool)\{Co^{II}(CH_3CN)\}_2]^{4+}$. This correlates with a change of π-donor ligands (μ-OH^-, Cl^-, Br^-) to a strong π-acceptor ligand (CH_3CN) in the axial positions. Hence, these transitions are diagnostic for the nature of the donors in the axial positions.

Electrochemical properties

Cyclic voltammograms were recorded on CH_3CN solutions of the dinuclear $Co^{II}Co^{II}$ complexes (Fig. 5). Peak potentials (Table 2) are referenced *versus* Fc^+/Fc used as internal standard. All complexes show irreversible oxidative and reductive processes that are influenced by the dinucleating and the exogenous ligands.

The effects on the redox processes differ for five- and six-coordinate complexes and will thus be discussed separately. The six-coordinate complex $[(susan^{6\text{-}Me})\{Co^{II}(CH_3CN)_2\}_2]^{4+}$ shows one oxidative process at 1.49 V that is probably a metal-centered oxidation to a $Co^{III}Co^{II}$ species, while the first oxidative process in the analogous $[(susan)\{Co^{II}(CH_3CN)_2\}_2]^{4+}$ is at 0.46 V. This cathodic shift of ∼1 V show that for octahedral coordination the Co^{III}/Co^{II} redox couple shifts as expected to lower potential with stronger σ-donors (susan *vs.* $susan^{6\text{-}Me}$). The doubly bridged complex $[(susan^{6\text{-}Me})\{Co^{II}(\mu\text{-}OH)_2Co^{II}\}]^{2+}$ shows two oxidative processes at 0.72 and 1.26 V, that evoke reductive back currents at 0.30 and −0.18 V, respectively. However, the overall charge differ to that of $[(susan^{6\text{-}Me})\{Co^{II}(CH_3CN)_2\}_2]^{4+}$ prohibiting a direct comparison of reduction potentials as reduction potentials generally increase by increasing positive charge of the complex according to the Born equation.[4,28]

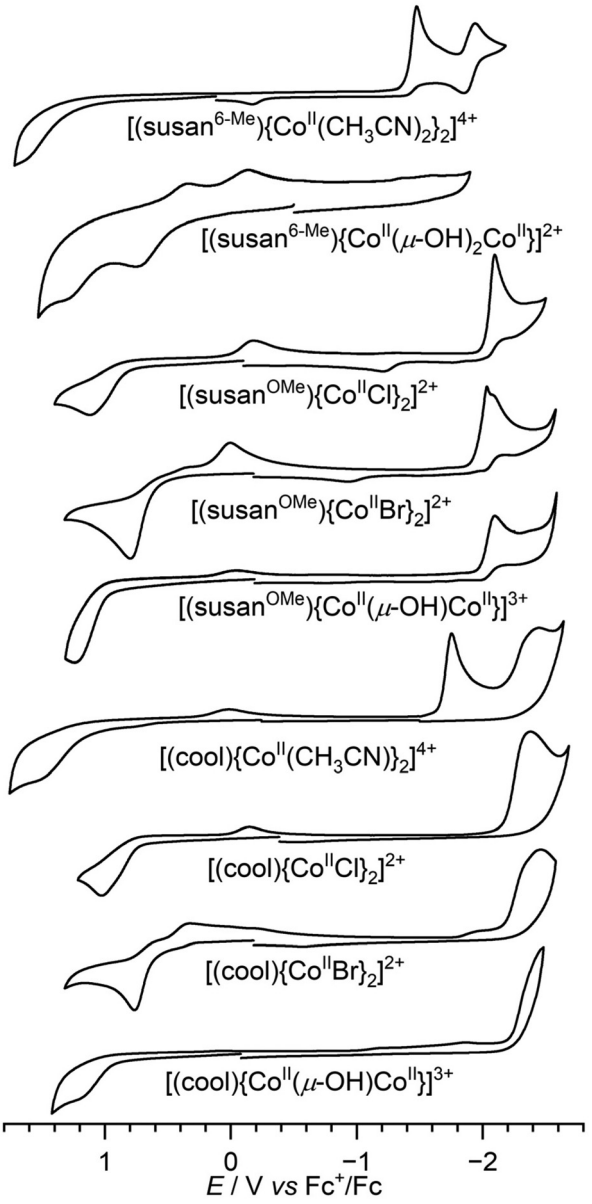

Fig. 5 Cyclic voltammograms of the dinuclear complexes in CH_3CN solutions containing 0.1 M $TBAPF_6$ as supporting electrolyte. Scan rate is 200 mV s^{-1}.

In the reductive part, both $[(susan^{6\text{-}Me})\{Co^{II}(CH_3CN)_2\}_2]^{4+}$ and $[(susan)\{Co^{II}(CH_3CN)_2\}_2]^{4+}$ show a reversible reduction at −1.9 V. This reduction was assigned to be ligand-centered in the complex with susan, while the higher potential reduction at −1.53 V was assigned to be metal-centered to a $Co^{II}Co^{I}$ species.[16] The shift of the latter to higher potential at −1.41 V in the complex with $susan^{6\text{-}Me}$ corroborates on the one hand the lower electron donation ability of $susan^{6\text{-}Me}$ than of susan as already observed in the oxidative processes and on the other hand the metal-centered assignment.

The five-coordinate complexes exhibit in the reductive part mostly the ligand-centered reduction that is not affected by the exogenous ligands. The trend −1.9 V (susan) > −2.1 V

(susan^{OMe}) > −2.4 V (cool) follows the expected trend of increasing electron density in the aromatic systems of susan < susan^{OMe} < cool. Furthermore, reductive processes to metal-centered $Co^{II}Co^{I}$ species at higher potentials are observed besides for [(cool){$Co^{II}(CH_3CN)$}$_2$]$^{4+}$ (−1.76 V) also for [(susan){$Co^{II}Br$}$_2$]$^{2+}$ (−1.83 V) and [(susan^{OMe}){$Co^{II}Br$}$_2$]$^{2+}$ (−2.03 V). The lower potential of [(susan^{OMe}){$Co^{II}Br$}$_2$]$^{2+}$ than of [(susan){$Co^{II}Br$}$_2$]$^{2+}$ demonstrates the higher electron donation of susan^{OMe} than of susan.

In the oxidative part, the nine five-coordinate complexes varying the ligand (susan, susan^{OMe}, cool) and the exogenous donors (Br^-, Cl^-, μ-OH^-) allow to study the individual contributions to the potential. Considering the variation of the exogenous donors, the potential generally increases in the order Br^- (0.75–0.79 V) < Cl^- (1.02–1.10 V) < μ-OH^- (1.18–1.31 V), which is counter-intuitive to the increasing electron donation ability of the donors in this series. This was rationalized in our study on the susan complexes[16] that the oxidation is from five-coordinate Co^{II} high-spin to six-coordinate Co^{III} low-spin. The latter has antibonding interaction with π-donor ligands so that the increasing π-donor ability Br^- < Cl^- < μ-OH^- destabilizes Co^{III} low-spin and hence increases the potential.

For the halide complexes, the variation of the potential by changing the dinucleating ligand is relatively small (Cl^-: 80 mV; Br^-: 40 mV). The strongest variation occurs in the {Co^{II}(μ-OH)Co^{II}} complexes with susan (1.31 V) > susan^{OMe} (1.24) > cool (1.18 V) in-line with the increasing electron donation ability susan < susan^{OMe} < cool.

Conclusions

The differences in the molecular structures of the dinuclear $Co^{II}Co^{II}$ complexes already allow conclusions to be drawn about the electron-donating ability of the ligands cool, susan, susan^{OMe}, and susan$^{6\text{-}Me}$. All complexes of the ligand cool are only five-coordinate including that with exogenous π-accepting CH_3CN demonstrating its strongest electron donation capability correlated with shorter Co–N^{im} than Co–N^{py} bond lengths in related trigonal-bipyramidally coordinated complexes with Cl^-, Br^-, and μ-OH^-. For the μ-OH^- complexes, only the ligand susan$^{6\text{-}Me}$ requires two μ-OH^- bridges resulting in six-coordinate Co^{II} ions, while the ligands cool, susan^{OMe}, and susan only include one μ-OH^- bridge and therefore five-coordinate Co^{II} ions. This shows that the ligand susan$^{6\text{-}Me}$ is less electron-donating due to the longer Co–$N^{6\text{-}Me\text{-}py}$ bonds than the Co–N^{py} bonds caused by the steric interference of the 6-Me groups oriented towards *cis*-coordinated ligands. Despite the longer Co–$N^{6\text{-}Me\text{-}py}$ bonds, the steric demand of the 6-Me groups enforces a facial coordination of the DPA-subunits in [(susan$^{6\text{-}Me}$){$Co^{II}(CH_3CN)_2$}$_2$]$^{4+}$, whereas in the otherwise analogous [(susan){$Co^{II}(CH_3CN)_2$}$_2$]$^{4+}$ the DPA-subunits are meridionally coordinated. Overall, the structural analysis provides the following sequence of electron donation capability: susan$^{6\text{-}Me}$ < susan^{OMe}/susan < cool without the possibility for a differentiation between susan^{OMe} and susan.

The magnetic data and the extracted spin-Hamiltonian parameters also show characteristic differences by varying the dinucleating and the exogenous ligands. For the complexes without a bridging hydroxo ligand, the zero-field splitting is much stronger for the six-coordinate complexes than for the five-coordinate complexes attributed to the stronger splitting of the octahedral $^4T_{1g}$ ground state by the trigonal bipyramidal coordination environment. There is no significant difference observed in the zero-field splittings for pyridine of imidazole donors. An important difference is the exchange coupling in the μ-hydroxo-bridged complexes, which is slightly ferromagnetic in the bis-μ-hydroxo bridged complex [(susan$^{6\text{-}Me}$){Co^{II}(μ-OH)$_2$$Co^{II}$}]$^{2+}$, but antiferromagnetic and stronger in the μ-hydroxo-bridged five-coordinate complexes.

The UV-Vis-NIR spectra exhibit specific trends in the d–d transitions. The complexes that are six-coordinate in the solid-state exhibit generally lower intensities in the solution d–d spectra than the complexes that are five-coordinate in the solid-state (a well-known observation due to lifting of the Laporte rule) confirming that their coordination number is retained upon dissolution. This is supported by a weak band around 9000 cm^{-1} in the six-coordinate complexes, while the five-coordinate complexes show a more intense band below 7000 cm^{-1}. The μ-hydroxo-bridged complexes show a unique band around 22 000–23 000 cm^{-1} confirming their bridged nature upon dissolution. Overall, all significant changes observed in the UV-Vis-NIR spectra can be interpreted consistently with changes in the solid-state structure providing strong evidence that the solid-state structures retain in solution. This will be a valuable tool for the study of the reactivity of these $Co^{II}Co^{II}$ complexes. Moreover, the spectral features in the range 15 000–22 000 cm^{-1} vary specifically for the complexes with cool compared to structural analogous complexes of susan and susan^{OMe} demonstrating the differing donor-strength of imidazole, while again no differentiation can be made between susan and susan^{OMe}.

The electrochemical characterization provides a large set of potentials that are dependent on the coordination number, the dinucleating ligand, and the exogenous donor. For the six-coordinate complexes, the oxidation is facilitated by stronger σ-donor and less π-acceptor character and demonstrates a much stronger electron-donation of susan than of susan$^{6\text{-}Me}$. In the five-coordinate complexes, the oxidation is counter-intuitively facilitated by less π-donation assigned to antibonding interactions of π-donors with Co^{III} low-spin. Irrespective of this, potentials for oxidations and reduction are shifted to lower potentials for susan^{OMe} than for susan (*e.g.* 200 mV cathodic shift for the reduction of [(susan^{OMe}){$Co^{II}Br$}$_2$]$^{2+}$ *vs.* [(susan){$Co^{II}Br$}$_2$]$^{2+}$) providing an experimental handle for its stronger electron donation ability.

Taking together the information obtained from all measurements, the overall electron donation ability has the order susan$^{6\text{-}Me}$ ≪ susan < susan^{OMe} ≪ cool. The +I effect of the 6-Me substituents is minor as the ligand-centered reduction is not affected. The strongly reduced electron donation of susan$^{6\text{-}Me}$ originates from the longer Co–$N^{6\text{-}Me\text{-}py}$

bond due to the sterical demand of the 6-Me groups. The stronger electron donation of susan^{OMe} than of susan originates from the higher electron density in the pyridine rings that reduces the π-acceptor character of the pyridine. This effect is not strong enough to influence bond lengths significantly but strong enough to influence redox potentials. On the other hand, the effect is strong going from susan/susan^{OMe} to cool with significantly shorter Co–N^{im} bonds demonstrate stronger Co–N^{im} bonds. This cannot be attributed to the change from a π-acceptor to a π-donor ligand[15] but indicates an increasing main σ-donor character of the imidazole than the pyridine donors resulting in an overall stronger electron donation. In summary, the new ligand cool is a significantly stronger electron donating member in our family of dinucleating ligands and the influence on stability and reactivity in peroxo and high-valent complexes is currently under study in our lab.

Data availability

The supplementary crystallographic data for this study have been deposited at the Cambridge Crystallographic Data Centre under accession codes 2341023–2341031.†

Author contributions

F. D. conducted the syntheses as well as the spectroscopic, magnetic, and electrochemical characterization. T. L. conducted the initial syntheses of the ligand cool and of some of the complexes. A. S., H. B., and J. O. collected, solved, and refined all the crystallographic data. T. G. designed experiments, assisted with data analysis, and wrote the manuscript with input from all the authors.

Conflicts of interest

The authors declare no competing financial interests.

Acknowledgements

The DFG (Research Unit FOR 5215 "Bioinspired Oxidation Catalysis with Iron Complexes "BioOxCat", TP1") and Bielefeld University are gratefully acknowledged for funding.

References

1 R. H. Holm, P. Kennepohl and E. I. Solomon, *Chem. Rev.*, 1996, **96**, 2239–2314.
2 (*a*) L. Que Jr. and W. B. Tolman, *Nature*, 2008, **455**, 333–340; (*b*) R. M. Bullock, J. G. Chen, L. Gagliardi, P. J. Chirik, O. K. Farha, C. H. Hendon, C. W. Jones, J. A. Keith, J. Klosin, S. D. Minteer, R. H. Morris, A. T. Radosevich, T. B. Rauchfuss, N. A. Strotman, A. Vojvodic, T. R. Ward, J. Y. Yang and Y. Surendranath, *Science*, 2020, **369**, eabc3183; (*c*) S. Sahu and D. P. Goldberg, *J. Am. Chem. Soc.*, 2016, **138**, 11410–11428; (*d*) Y. Liang, J. Wei, X. Qiu and N. Jiao, *Chem. Rev.*, 2018, **118**, 4912–4945; (*e*) A. J. Jasniewski and L. Que, *Chem. Rev.*, 2018, **118**, 2554–2592; (*f*) C. E. Elwell, N. L. Gagnon, B. D. Neisen, D. Dhar, A. D. Spaeth, G. M. Yee and W. B. Tolman, *Chem. Rev.*, 2017, **117**, 2059–2107; (*g*) E. Y. Tshuva and S. J. Lippard, *Chem. Rev.*, 2004, **104**, 987–1012.
3 (*a*) T. Glaser, *Coord. Chem. Rev.*, 2019, **380**, 353–377; (*b*) S. Walleck and T. Glaser, *Isr. J. Chem.*, 2020, **60**, 1019–1031.
4 J. B. H. Strautmann, S. Walleck, H. Bögge, A. Stammler and T. Glaser, *Chem. Commun.*, 2011, **47**, 695–697.
5 J. B. H. Strautmann, S. Dammers, T. Limpke, J. Parthier, T. P. Zimmermann, S. Walleck, G. Heinze-Brückner, A. Stammler, H. Bögge and T. Glaser, *Dalton Trans.*, 2016, **45**, 3340–3361.
6 S. Walleck, T. P. Zimmermann, H. Hachmeister, C. Pilger, T. Huser, S. Katz, P. Hildebrandt, A. Stammler, H. Bögge, E. Bill and T. Glaser, *Nat. Commun.*, 2022, **13**, 1376.
7 T. P. Zimmermann, N. Orth, S. Finke, T. Limpke, A. Stammler, H. Bögge, S. Walleck, I. Ivanović-Burmazović and T. Glaser, *Inorg. Chem.*, 2020, **59**, 15563–15569.
8 L. Siebe, C. Butenuth, A. Stammler, H. Bögge, S. Walleck and T. Glaser, *Inorg. Chem.*, 2024, **63**, 2627–2639.
9 F. Depenbrock, T. Limpke, E. Bill, D. J. SantaLucia, M. van Gastel, S. Walleck, J. Oldengott, A. Stammler, H. Bögge and T. Glaser, *Inorg. Chem.*, 2023, **62**, 17913–17930.
10 (*a*) J. B. Gordon, A. C. Vilbert, M. A. Siegler, K. M. Lancaster, P. Moënne-Loccoz and D. P. Goldberg, *J. Am. Chem. Soc.*, 2019, **141**, 3641–3653; (*b*) A. Chandra, M. Ansari, I. Monte-Pérez, S. Kundu, G. Rajaraman and K. Ray, *Angew. Chem., Int. Ed.*, 2021, **60**, 14954–14959; (*c*) M. S. Møller, J. Kongsted and C. J. McKenzie, *Dalton Trans.*, 2021, **50**, 4819–4829; (*d*) Z.-Y. Chen, Z.-H. Long, X.-Z. Wang, J.-Y. Zhou, X.-S. Wang, X.-P. Zhou and D. Li, *Inorg. Chem.*, 2021, **60**, 10380–10386; (*e*) A. A. DeLucia, K. A. Kelly, K. A. Herrera, D. L. Gray and L. Olshansky, *Inorg. Chem.*, 2021, **60**, 15599–15609; (*f*) M. K. Goetz, J. E. Schneider, A. S. Filatov, K. A. Jesse and J. S. Anderson, *J. Am. Chem. Soc.*, 2021, **143**, 20849–20862; (*g*) P. Kumar, L. Devkota, M. C. Casey, A. A. Fischer, S. V. Lindeman and A. T. Fiedler, *Inorg. Chem.*, 2022, **61**, 16664–16677; (*h*) J. Amtawong, A. I. Nguyen and T. D. Tilley, *J. Am. Chem. Soc.*, 2022, **144**, 1475–1492; (*i*) W. Mao, D. Fehn, F. W. Heinemann, A. Scheurer, M. van Gastel, S. A. V. Jannuzzi, S. DeBeer, D. Munz and K. Meyer, *Angew. Chem., Int. Ed.*, 2022, **61**, e202206848; (*j*) Y.-F. Su, W.-Z. Luo, W.-Q. Lin, Y.-B. Su, Z.-J. Li, Y.-J. Yuan, J.-F. Li, G.-H. Chen, Z. Li, Z.-T. Yu and Z. Zou, *Angew. Chem., Int. Ed.*, 2022, **61**, e202201430; (*k*) J. B. Gordon, T. Albert, S. Yadav, J. Thomas, M. A. Siegler, P. Moënne-Loccoz and D. P. Goldberg, *Inorg. Chem.*, 2023, **62**, 392–400; (*l*) N. Zhao, M. K. Goetz, J. E. Schneider and J. S. Anderson, *J. Am. Chem. Soc.*, 2023, **145**, 5664–5673; (*m*) A. A. DeLucia and L. Olshansky, *Inorg. Chem.*, 2024, **63**, 1109–1118.

11 L. P. Hammett, *J. Am. Chem. Soc.*, 1937, **59**, 96–103.
12 (*a*) J. B. H. Strautmann, C.-G. Freiherr von Richthofen, G. Heinze-Brückner, S. DeBeer, E. Bothe, E. Bill, T. Weyhermüller, A. Stammler, H. Bögge and T. Glaser, *Inorg. Chem.*, 2011, **50**, 155–171; (*b*) J. B. H. Strautmann, C.-G. Freiherr von Richthofen, S. DeBeer George, E. Bothe, E. Bill and T. Glaser, *Chem. Commun.*, 2009, 2637–2639.
13 S. Finke, A. Stammler, J. Oldengott, S. Walleck and T. Glaser, *Dalton Trans.*, 2023, **52**, 17548–17561.
14 G. Xue, D. Wang, R. de Hont, A. T. Fiedler, X. Shan, E. Münck and L. Que Jr., *Proc. Natl. Acad. Sci. U. S. A.*, 2007, **104**, 20713–20718.
15 R. J. Sundberg, R. F. Bryan, I. F. Taylor and H. Taube, *J. Am. Chem. Soc.*, 1974, **96**, 381–392.
16 F. Depenbrock, T. Limpke, A. Stammler, J. Oldengott, H. Bögge and T. Glaser, *Eur. J. Inorg. Chem.*, 2022, e202100992.
17 W. L. F. Armarego and C. L. L. Chai, *Purification of laboratory chemicals*, Elsevier/Butterworth-Heinemann, Amsterdam, Boston, 6th edn, 2009.
18 M. F. Braña, J. M. Castellano, D. Perron, C. Maher, D. Conlon, P. F. Bousquet, J. George, X.-D. Qian and S. P. Robinson, *J. Med. Chem.*, 1997, **40**, 449–454.
19 S. Dammers, T. P. Zimmermann, S. Walleck, A. Stammler, H. Bögge, E. Bill and T. Glaser, *Inorg. Chem.*, 2017, **56**, 1779–1782.
20 *SADABS*, Bruker AXS Inc., Madison, Wisconsin, USA, 2021.
21 (*a*) G. M. Sheldrick, *Acta Crystallogr., Sect. A: Found. Crystallogr.*, 2008, **64**, 112–122; (*b*) G. M. Sheldrick, *Acta Crystallogr., Sect. A: Found. Adv.*, 2015, **71**, 3–8.
22 G. M. Sheldrick, *Acta Crystallogr., Sect. C: Struct. Chem.*, 2015, **71**, 3–8.
23 A. L. Spek, *Acta Crystallogr., Sect. C: Struct. Chem.*, 2015, **71**, 9–18.
24 O. V. Dolomanov, L. J. Bourhis, R. J. Gildea, J. A. K. Howard and H. Puschmann, *J. Appl. Crystallogr.*, 2009, **42**, 339–341.
25 A. F. Abdel-Magid, K. G. Carson, B. D. Harris, C. A. Maryanoff and R. D. Shah, *J. Org. Chem.*, 1996, **61**, 3849–3862.
26 (*a*) C. He and S. J. Lippard, *Inorg. Chem.*, 2001, **40**, 1414–1420; (*b*) J. Kuzelka, S. Mukhopadhyay, B. Spingler and S. J. Lippard, *Inorg. Chem.*, 2003, **42**, 6447–6457; (*c*) S. V. Kryatov, S. Taktak, I. V. Korendovych, E. V. Rybak-Akimova, J. Kaizer, S. Torelli, X. Shan, S. Mandal, V. L. MacMurdo, A. Mairata i Payeras and L. Que, *Inorg. Chem.*, 2005, **44**, 85–99; (*d*) F. L. B. Röhs, S. Dammers, A. Stammler, J. Oldengott, H. Bögge, E. Bill and T. Glaser, *Eur. J. Inorg. Chem.*, 2022, **2022**, e202200177.
27 The program package JulX was used for spin-Hamiltonian simulations and fittings of the data by a full-matrix diagonalization approach (E. Bill, unpublished results).
28 (*a*) M. Born, *Z. Phys.*, 1920, **1**, 45–48; (*b*) T. Beissel, F. Birkelbach, E. Bill, T. Glaser, F. Kesting, C. Krebs, T. Weyhermüller, K. Wieghardt, C. Butzlaff and A. X. Trautwein, *J. Am. Chem. Soc.*, 1996, **118**, 12376–12390; (*c*) T. Glaser, M. Heidemeier, J. B. H. Strautmann, H. Bögge, A. Stammler, E. Krickemeyer, R. Huenerbein, S. Grimme, E. Bothe and E. Bill, *Chem. – Eur. J.*, 2007, **13**, 9191–9206.
29 A. W. Addison, T. N. Rao, J. Reedijk, J. van Rijn and G. C. Verschoor, *J. Chem. Soc., Dalton Trans.*, 1984, 1349–1356.